CHEMMEDCHEM

DOI: 10.1002/cmdc.201000101

Synthesis, 3D-QSAR, and Structural Modeling of Benzolactam Derivatives with Binding Affinity for the D_2 and D_3 Receptors

Laura López,[a] Jana Selent,[a] Raquel Ortega,[b] Christian F. Masaguer,[b] Eduardo Domínguez,[c] Filipe Areias,[c] José Brea,[c] María Isabel Loza,[c] Ferran Sanz,[a] and Manuel Pastor*[a]

A series of 37 benzolactam derivatives were synthesized, and their respective affinities for the dopamine D_2 and D_3 receptors evaluated. The relationships between structures and binding affinities were investigated using both ligand-based (3D-QSAR) and receptor-based methods. The results revealed the importance of diverse structural features in explaining the differences in the observed affinities, such as the location of the benzolactam carbonyl oxygen, or the overall length of the compounds. The optimal values for such ligand properties are slightly different for the D_2 and D_3 receptors, even though the binding sites present a very high degree of homology. We explain these differences by the presence of a hydrogen bond network in the D_2 receptor which is absent in the D_3 receptor and limits the dimensions of the binding pocket, causing residues in helix 7 to become less accessible. The implications of these results for the design of more potent and selective benzolactam derivatives are presented and discussed.

Introduction

The dopamine neurotransmitter is known to play a key role in numerous physiological and pathophysiological processes. In the brain, dopamine receptors are expressed in distinct but overlapping areas, and are involved in the regulation of functions such as motion, emotion, and cognition. Dopamine receptors can be divided into five different receptor subtypes, organized into two families based on whether their effect on adenylate cyclase is stimulation (D_1-like family, D_1 and D_5) or inhibition (D_2-like family, D_2, D_3 and D_4).[1,2]

Structurally, dopamine receptors belong to the class A rhodopsin-like G-protein-coupled receptors (GPCRs) and are composed of seven transmembrane (TM) helices connected by three intracellular (ICL) and extracellular (ECL) loops. Most of the primary sequence homology among the different groups of GPCRs is found within the TM domains.

The dopamine D_2 receptor is the primary pharmacological target for classic antipsychotic drugs such as haloperidol, which is presumed to decrease positive symptoms of schizophrenia through D_2 receptor blockade in the mesolimbic area. Unfortunately, they are also responsible for the extrapyramidal side effects (EPS) of these compounds, mediated through D_2 blockade in the dorsal striatum. Atypical antipsychotic drugs such as clozapine, which is still considered the gold standard among antipsychotic drugs because of the absence of associated EPS, also exhibits binding affinity for the D_2 receptor. However, abundant experimental evidence demonstrates that D_2 binding affinity alone does not explain the therapeutic effect of most antipsychotic drugs; therefore, a large effort has been invested in the search of alternative biological targets that could be used for the design of safe and effective antipsychotic drugs. Among these, the D_3 receptor appears a promising target.

The dopamine D_3 receptor was cloned almost two decades ago[3] and is structurally very similar to the D_2 receptor, with a sequence identity of 78% and a sequence similarity of 88% in the regions putatively involved in ligand recognition (Gonnet250 similarity matrix).[4] However, the D_3 receptor is generally less abundant than the D_2 receptor, and this difference is particularly striking in the caudate and putamen.[5] Postmortem studies of schizophrenic patients have shown an increase in D_3 receptor levels in the nucleus accumbens[6] as well as a decrease in parietal and motor cortex.[7] Moreover, further data suggest that most antipsychotic drugs have considerable affinity for the D_3 receptor[3,8] and that the D_3 antagonism ameliorates the EPS and cognitive symptoms.[9,10]

For the aforementioned reasons it is of interest to obtain D_3-receptor-selective compounds in order to explore the true anti-

[a] L. López, Dr. J. Selent, Dr. F. Sanz, Dr. M. Pastor
Research Programme on Biomedical Informatics (GRIB), IMIM, DCEXS
Universitat Pompeu Fabra, Dr. Aiguader 88, 08003 Barcelona (Spain)
Fax: (+34) 933160550
E-mail: manuel.pastor@upf.edu

[b] R. Ortega, Dr. C. F. Masaguer
Departamento de Química Orgánica, Facultad de Farmacia
Universidad de Santiago de Compostela, 15782
Santiago de Compostela (Spain)

[c] Dr. E. Domínguez, Dr. F. Areias, Dr. J. Brea, Dr. M. I. Loza
Departamento de Farmacología
Instituto de Farmacia Industrial, Facultad de Farmacia
Universidad de Santiago de Compostela, 15782
Santiago de Compostela (Spain)

psychotic potential of this receptor and to distinguish these pharmacological effects from those mediated by the D_2 receptor. For instance, recent work by Millan et al. showed preferential binding of compound S33138 to the D_3 receptor over the D_2 receptor, a binding profile which is associated with preservation of cognitive function. This compound is now in phase IIb clinical trials for treatment of schizophrenia.[11]

However, the high degree of homology between the D_2 and D_3 receptors makes it difficult to obtain selective compounds, although a few series of compounds exhibiting some degree of selectivity have been published.[12–14] In a recent short paper,[14] we described a series of 26 benzolactam derivatives containing a benzolactam and an arylpiperazine ring, linked by a propyl or butyl chain, which exhibit affinity for the D_2 and D_3 receptors. Structure–activity relationship (SAR) studies of this series concluded that both the length of the linker between the lactam and the piperazine ring, as well as the size of the lactam ring, influenced their D_2 and D_3 affinities.

In the work presented herein, we pursue an in-depth analysis of the binding of these compounds to both the D_2 and D_3 receptors with the aim of identifying structural properties linked to the previously observed selectivity that may be suitable for enhancement to yield new derivatives with better selectivity for the D_3 versus D_2 receptor. As a starting point for this analysis, we synthesized a series of 12 novel benzolactam derivatives (Table 2), extending the series originally reported by Ortega et al.[14] (Table 1) that exhibits a wide range of affinities for the D_2 and D_3 receptors. All of the compounds in these series were submitted to docking simulations using homology models of D_2 and D_3 receptors. The docked ligand structures were used to build 3D-QSAR models describing the association between ligand structural features and their binding and selectivity properties. The obtained results were compared with previously reported SAR and structural analyses of the ligand–receptor complexes, evaluating their potential application for the design of potent and selective D_3 receptor derivatives.

Results and Discussion

Chemistry

The synthetic route for the preparation of the target arylpiperazinylalkylbenzolactams started from a commercially available benzocycloalkanone (1-indanone or 1-tetralone), with the aim of achieving the corresponding benzolactam by a Schmidt rearrangement (Scheme 1). The Schmidt reaction, according to published results, gives the benzolactam **3** as the major product; however, by changing the reaction medium from trichloroacetic acid,[15] polyphosphoric acid,[16] or sulfuric acid[17] to concentrated hydrochloric acid,[18] the desired benzolactam

Table 1. Human D_2 and D_3 receptor binding affinities for benzolactam derivatives of scaffolds A and B.[a]

Scaffold A:

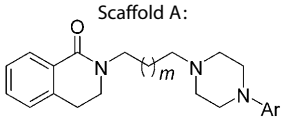

Scaffold B:

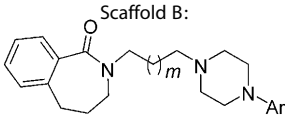

Compd	Code	Scaffold	*m*	Structure Ar	D_2	D_3	pK_i Ratio D_3/D_2
5a	USC-A301	A	1	2-methoxyphenyl	50.42% ±2.80 (2)	5.80±0.15 (3)	6.31
5b	USC-A302	A	1	4-methoxyphenyl	1.35% ±6.95 (2)	5.00±0.37 (3)	>1000
5c	USC-A303	A	1	2-pyridyl	12.40% ±0.52 (2)	5.08±0.11 (3)	>1000
5d	USC-A304	A	1	2-pyrimidyl	0.36% ±6.95 (2)	4.61±0.20 (3)	>1000
5e	USC-A305	A	1	3-trifluoromethylphenyl	52.38% ±0.73 (2)	5.62±0.24 (3)	4.17
5f	USC-A306	A	1	2,3-dichlorophenyl	59.87% ±4.77 (2)	6.68±0.49 (3)	47.86
6a	USC-B301	B	1	2-methoxyphenyl	6.10±0.07 (3)	6.68±0.16 (3)	3.80
6b	USC-B302	B	1	4-methoxyphenyl	1.10% ±11.51 (2)	5.96±0.34 (3)	>1000
6c	USC-B303	B	1	2-pyridyl	26.26% ±0.00 (2)	5.38±0.32 (3)	>1000
6d	USC-B304	B	1	2-pyrimidyl	36.44% ±0.31 (2)	5.08±0.32 (3)	380.19
6e	USC-B305	B	1	3-trifluoromethylphenyl	55.46% ±0.62 (2)	5.98±0.18 (3)	9.55
6f	USC-B306	B	1	2,3-dichlorophenyl	6.66±0.05 (3)	6.41±0.14 (3)	0.56
12a	USC-A401	A	2	2-methoxyphenyl	7.91±0.30 (3)	8.58±0.16 (3)	4.68
12b	USC-A402	A	2	4-methoxyphenyl	33.25% ±2.59 (2)	6.31±0.19 (3)	>1000
12c	USC-A403	A	2	2-pyridyl	57.54% ±0.31 (2)	7.92±0.21 (3)	>1000
12d	USC-A404	A	2	2-pyrimidyl	60.51% ±0.12 (2)	5.82±0.12 (3)	6.61
12f	USC-A406	A	2	2,3-dichlorophenyl	7.94±0.52 (3)	6.79±0.26 (3)	0.07
12g	USC-A407	A	2	2-chlorophenyl	7.45±0.10 (3)	8.17±0.16 (3)	5.25
12h	USC-A408	A	2	3-methoxyphenyl	6.80±0.11 (3)	7.39±0.14 (3)	3.89
13a	USC-A501	A	3	2-methoxyphenyl	7.69±0.09 (3)	7.49±0.18 (3)	0.63
14a	USC-B401	B	2	2-methoxyphenyl	8.44±0.17 (3)	8.80±0.35 (3)	2.29
14b	USC-B402	B	2	4-methoxyphenyl	59.02% ±0.73 (2)	7.39±0.08 (3)	245.47
14c	USC-B403	B	2	2-pyridyl	6.64±0.05 (3)	6.40±0.21 (3)	0.58
14d	USC-B404	B	2	2-pyrimidyl	6.82±0.24 (3)	6.20±0.16 (3)	0.24
14f	USC-B406	B	2	2,3-dichlorophenyl	7.44±0.07 (3)	7.84±0.17 (3)	2.51

[a] Binding affinities are shown as pK_i or percent displacement at 10 μM; all values are the mean of two or three separate competition experiments, and the number of assays conducted for each compound is reported in parentheses.

Table 2. Human D_2 and D_3 receptor binding affinities for benzolactam derivatives of scaffolds D and E.[a]

Scaffold D:

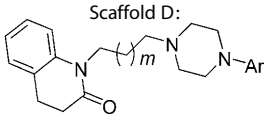

Scaffold E:

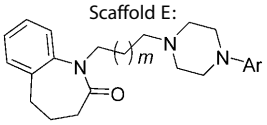

Compd	Code	Scaffold	*m*	Structure Ar	D_2	D_3	pK_i Ratio D_3/D_2
7a	USC-D301	D	1	2-methoxyphenyl	7.80 ± 0.18 (3)	6.35 ± 0.26 (3)	0.04
7b	USC-D302	D	1	4-methoxyphenyl	24.41 % ± 1.56 (2)	4.90 ± 0.35 (3)	> 1000
7c	USC-D303	D	1	2-pyridyl	50.92 % ± 0.31 (2)	5.29 ± 0.11 (3)	1.95
7d	USC-D304	D	1	2-pyrimidyl	50.55 % ± 3.32 (2)	5.04 ± 0.43 (3)	1.10
7f	USC-D306	D	1	2,3-dichlorophenyl	6.53 ± 0.10 (3)	6.20 ± 0.19 (3)	0.47
8a	USC-E301	E	1	2-methoxyphenyl	7.14 ± 0.13 (3)	6.57 ± 0.22 (3)	0.26
8f	USC-E306	E	1	2,3-dichlorophenyl	5.64 ± 0.06 (3)	5.10 ± 0.38 (3)	0.29
15a	USC-D401	D	2	2-methoxyphenyl	6.93 ± 0.11 (3)	7.45 ± 0.16 (3)	3.31
15b	USC-D402	D	2	4-methoxyphenyl	34.50 % ± 1.73 (2)	5.59 ± 0.11 (3)	> 1000
15c	USC-D403	D	2	2-pyridyl	57.14 % ± 8.78 (2)	6.08 ± 0.25 (3)	12.02
15d	USC-D404	D	2	2-pyrimidyl	59.06 % ± 5.99 (2)	5.63 ± 0.19 (3)	4.27
15f	USC-D406	D	2	2,3-dichlorophenyl	6.71 ± 0.14 (3)	6.39 ± 0.24 (3)	0.48

[a] Binding affinities are shown as pK_i or percent displacement at 10 μM; all values are the mean of two or three separate competition experiments, and the number of assays conducted for each compound is reported in parentheses.

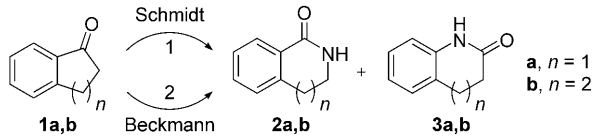

Scheme 1. Synthesis of benzolactams **2a**,**b** and **3a**,**b**. Reagents and conditions: 1) NaN_3 (2 equiv), HCl (conc.); 2) a) $NH_2OH{\cdot}HCl$, 4 N NaOH, MeOH, −10 °C → RT; b) TsCl, 4 N NaOH, acetone, −10 °C → RT; c) $AlCl_3$, CH_2Cl_2, −40 °C → RT.

2 can be obtained in moderate yield (42 %). This reaction was optimized by adding two equivalents of sodium azide,[19] which resulted in a 75–87 % yield of benzolactam **2** (Table 3).

Table 3. Yield values of benzolactams by two reaction methods.[a]

Compd	*n*	Method	**2** [%]	**3** [%]
1a	1	1	75	10
1a	1	2	5	60
1b	1	1	87	7
1b	2	2	5	85

[a] Method 1: Schmidt rearrangement; method 2: Beckmann rearrangement (see Scheme 1).

The Beckmann rearrangement, via oxime formation, led to the 2(1*H*) isomers of the benzolactam **3** as major compounds. A recent approximation of this reaction, through toluenesulfonylation of the oxime intermediate and subsequent catalysis with aluminum chloride, as shown in Scheme 1, produced the desired compounds **3a** or **3b** in 60 and 85 % yield, respectively.

Depending on the length of the spacer, one of two synthetic routes was used, originating from benzolactams **2a**–**b**, as shown in Scheme 2. In the case of a propyl spacer (Method A), chlorides **4a**–**f** were prepared from commercially available piperazines by alkylation with 1-bromo-3-chloropropane in acetone using 25 % aqueous NaOH as a base. The corresponding *N*-(3-chloropropyl)piperazines **4a**–**f** were obtained with 60–80 % yields. Alkylation of the benzolactams **2a**–**b** was achieved by treatment with chloropropylpiperazines **4a**–**f** in anhydrous benzene following deprotonation with NaH, resulting in the final compounds **5a**–**f** and **6a**–**f** in 60–85 % yields. Similarly, alkylation of the benzolactams **3a**–**b** with chloropropylpiperazines **4a**–**f** gave the desired products **7a**–**d**, **7f**, **8a**, and **8f** in 42–71 % yields.

Alkylation of N-substituted piperazines with 1-bromo-4-chlorobutane or 1-bromo-5-chloropentane, following Method A (Scheme 2), produced azaspiroazonium salts. Although the reaction of these salts with imides has been described,[20] in our case the desired products were obtained in very low yields. Consequently, Method B (Scheme 2) was used for the synthesis of *N*-arylpiperazinylbutyl and -pentyl benzolactams. Alkylation of benzolactams **2a**–**b** and **3a** with 1-bromo-4-chlorobutane or 1-bromo-5-chloropentane in anhydrous benzene using sodium hydride as a base provided the corresponding amides **9**–**11** in 59–75 % yield, depending on the size of the benzolactam ring.[21] For alkylation of piperazines, the best results were obtained by reaction of the arylpiperazine with the chloroalkylbenzolactam using potassium carbonate as a base and potassium iodide as a catalyst in methylisobutylketone. The alkylated benzolactams **12a**–**d**, **12f**–**h**, **13a**, **14a**–**d**, **14f**, **15a**–**d**, and **15f** were obtained in 30–75 % yields.

Structure–activity relationship analysis

The chemical structures and pharmacological data of the series under study are shown in Table 1 and Table 2. The general structure of the compounds (see Figure 1) is characterized by a benzolactam scaffold (fragment II), attached by an alkyl spacer to the nitrogen atom of a piperazine ring, while the opposite

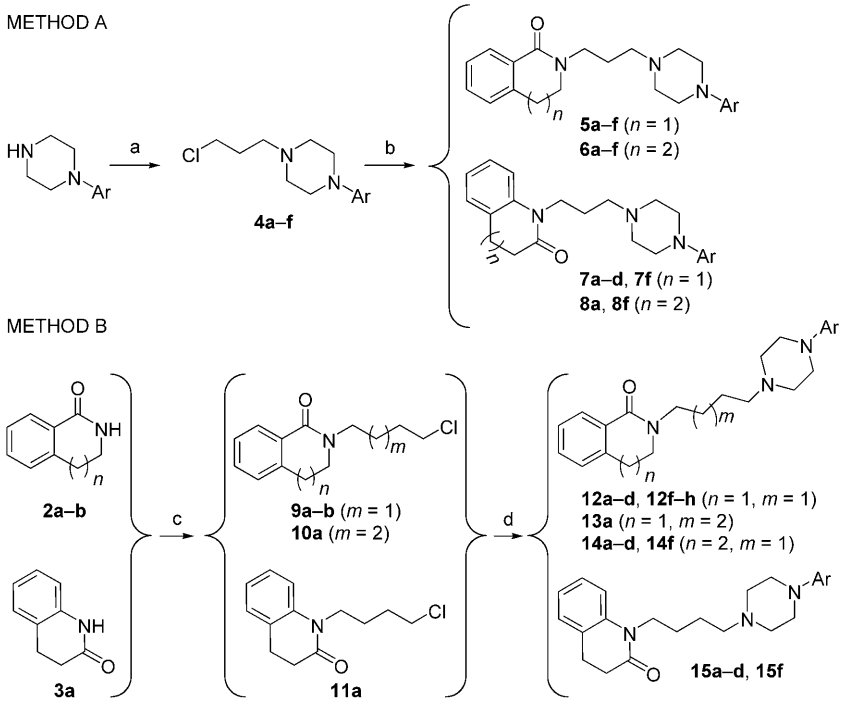

Scheme 2. Synthesis of *N*-(arylalkyl)benzolactams. Reagents and conditions: a) 1-bromo-3-chloropropane, NaOH, acetone; b) **2** or **3**, NaH, benzene, reflux; c) 1-bromo-4-chlorobutane or 1-bromo-5-chloropentane, NaH, benzene, reflux; d) arylpiperazine, K_2CO_3, KI, methyl isobutylketone, reflux.

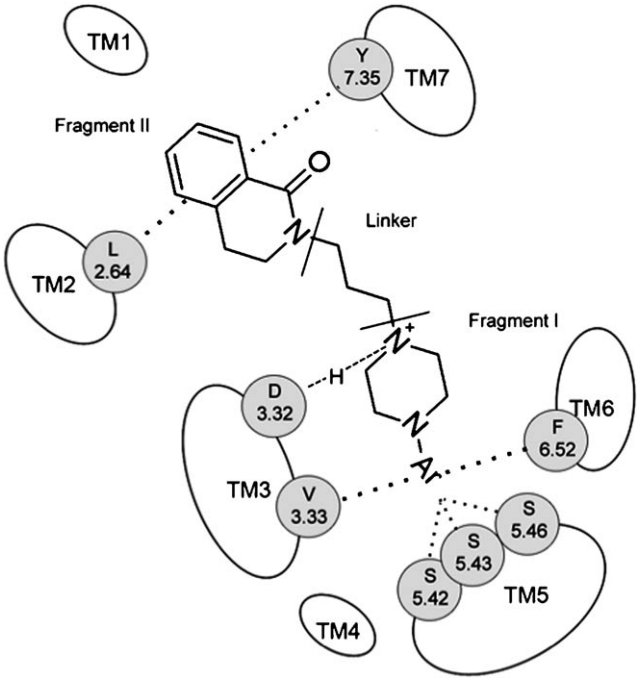

Figure 1. General structure of the benzolactam compounds and their key interactions with the D_2 and D_3 receptors.

piperazine nitrogen is linked to a variety of aryl substituents (fragment I). According to the obtained ligand–receptor complexes, these compounds bind to the same pocket in both the D_2 and D_3 receptors. The most important interactions, shown in Figure 1, are in agreement with our previous works:[14,22] 1) the well known salt bridge (Asp3.32) is essential for ligand binding, 2) the hydrophobic sandwich created by Val3.33 and Phe6.52 stabilizes the aryl ring of fragment I, 3) the serine residues of TM5 interact with the aryl substituents, and 4) the hydrophobic interactions with Leu2.64 and Tyr7.35 stabilize the benzolactam ring in fragment II.

The compounds in Table 1 exhibit binding affinities for D_2 and D_3 receptors in the micromolar range (pK_i for D_2 receptor: 4.5–8.4; pK_i for D_3 receptor: 4.6–8.8). Some of the compounds demonstrate selectivity for one of the receptors (e.g., compound **12 f** shows higher binding affinity for the D_2 receptor, while **12 c** has more binding affinity for the D_3 receptor). The observation of the structures and activities of the series in Table 1 follows some of the trends we have previously reported[14] that are worth summarizing here. Firstly, the length of the linker between the lactam and the piperazine rings affects the affinity of the compounds: derivatives with a propyl linker, such as **6 a** or **6 f** which have modest affinities for D_2 and D_3 receptors, become high affinity ligands when transformed into analogues with a butyl linker, such as **14 a** or **14 f**. Moreover, these compounds with a butyl linker are, in general, more selective for D_3. Transferring the methoxy group from position 2 to 4 (e.g., **12 a** to **12 b**; **14 a** to **14 b**) results in a decrease in affinity for D_2 and D_3 receptors while increasing selectivity toward the D_3 receptor over the D_2 receptor. Finally, increasing the size of the benzolactam from a six- to a seven-membered ring (scaffold A to scaffold B) slightly enhances affinities for the D_2 and D_3 receptors.

The new compounds included in the series (Table 2) follow the same trends, in particular the effects resulting from variations of the linker length and methoxy group position. These new compounds contain benzolactam ring scaffolds (scaffolds D and E) which only differ from the previous series (scaffolds A and B) by an isomeric alteration of the lactam structure due to a change in the position of the nitrogen (seen in a comparison between Tables 1 and 2). This seemingly small change is deemed detrimental for D_3/D_2 receptor selectivity, as it produces compounds with generally lower D_3 receptor affinities and slightly higher D_2 receptor affinities. Additionally, this alteration inverts the trend observed in the previous series with regard to how benzolactam ring size correlates with binding affinity. Therefore, in the isolactam series (Table 2), an increase in lactam ring size from six-membered (scaffold D, com-

pounds **7a** and **7f**) to seven-membered (scaffold E, compounds **8a** and **8f**) decreases rather than enhances affinity for both receptors.[14]

These collective observations, although significant, cannot be directly exploited for the purpose of designing compounds with a higher selectivity or D_3 receptor affinity than those already reported in Table 1 and Table 2. Rather, our intention is to pursue an understanding of the structural properties of the series that are responsible for the observed differences in binding affinity and selectivity, with the final aim of using this knowledge for the design and synthesis of improved compounds. 3D-QSAR methods are especially well suited for this purpose, as the resulting models can be used to identify structural features of the compounds which correlate to their binding affinities. For this study, we built ligand–receptor complexes between all compounds in the series and the receptors under study, using the obtained docking geometries (poses) as input for 3D-QSAR modeling. The reason for using this approach is twofold: Firstly, the docking poses are more representative of the bioactive conformations of the ligands than simpler extended conformations. Secondly, models obtained from analysis of the ligands can be compared with receptor structures to identifying ligand interactions or receptor residues that are critical for binding. The use of 3D-QSAR in these studies has an advantage over standard structure-based drug design (SBDD) methods in that it provides an objective assessment of the relevance of specific ligand–receptor interactions with respect to pharmacological properties, instead of allowing researchers to make these decisions subjectively.

For 3D-QSAR modeling, we decided to use GRIND-2,[23] the newest generation of GRIND,[24] as described below in the Experimental Section, because it provides a compromise between the quality of the compound description and the simplicity of application and interpretation. It should be noted that this is the first application of the novel CLACC algorithm (see Experimental Section for details), which improves greatly the interpretability and the predictive ability of GRIND.[24]

3D-QSAR model for D_2 receptor affinity

The initial 3D-QSAR model was built as described in the Experimental Section, using binding affinity values for the D_2 receptor that span 3.4 log units (from 5 to 8.4). The final partial least squares (PLS) model obtained after two sequential steps of fractional factorial design (FFD) variable selection contains 273 variables, and shows optimum predictive ability with three latent variables (LVs; Model M1, Table 4). Model M1 is of remarkably good quality, both in terms of fitting (r^2) and predictive ability (q^2). Therefore, we expected that interpretation of the most relevant variables in the model could be used to identify structural features important for D_2 receptor binding affinity. Visual analysis of the PLS coefficient plot (Figure 2a) allowed us to translate this information into a set of ligand structural features associated with either an increase or decrease in binding affinities. For the purpose of brevity, we will herein group those variables belonging to different correlograms, but representing the same ligand features.

Table 4. Statistical parameters of the described 3D-QSAR models.

Model	Num. LV[a]	Num. var.	r^{2}[b]	q^{2}_{LOO}[c]
M1	3	273	0.94	0.63
M2	3	279	0.97	0.82
M3	2	241	0.90	0.59

[a] Optimum number of LV found by leave-one-out (LOO) cross-validation. [b] Coefficient of determination. [c] LOO cross-validated coefficient of determination.

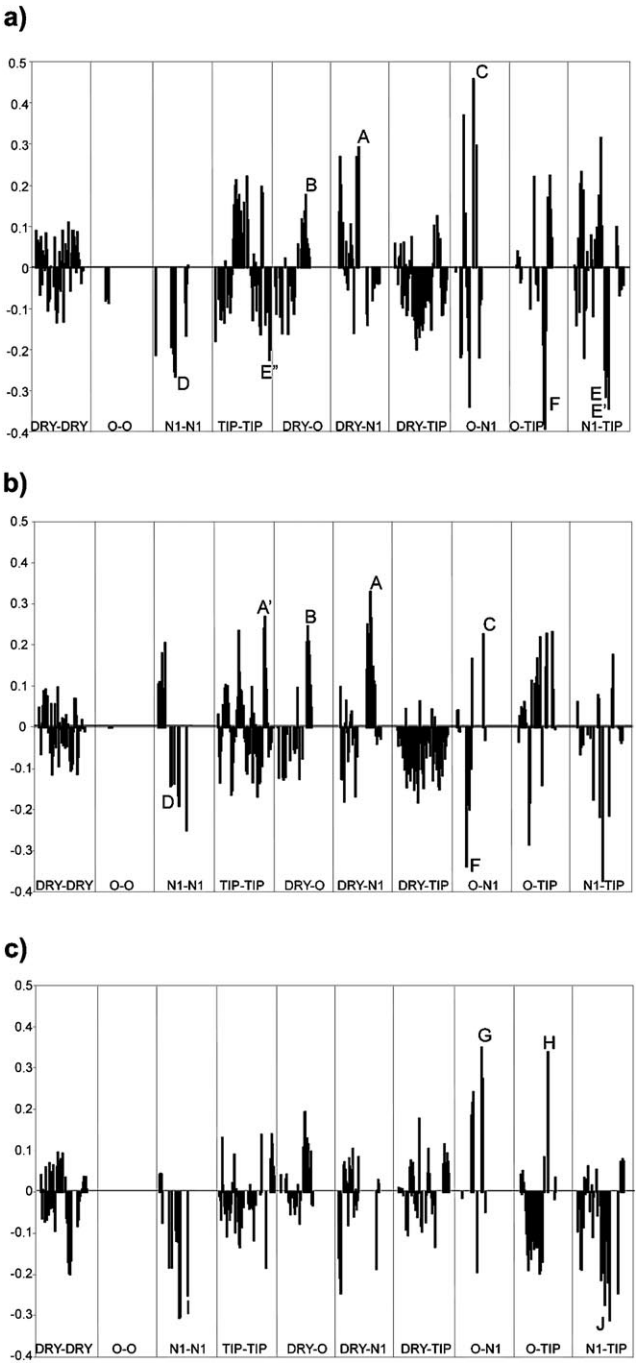

Figure 2. PLS coefficients obtained for a) model M1, b) model M2, and c) model M3.

In model M1, a number of variables with the highest positive coefficients, labeled as A, B, and C in Figure 2a, represent differing abilities of the compounds to place fragment II in a favorable situation. This includes having the aromatic moiety surrounded by hydrophobic residues, such as Leu2.64, Tyr7.35, and Ile183, and enabling the benzolactam carbonyl group to be positioned such that it can establish hydrogen bond interactions with the polar groups of helix seven, in this case, Thr7.39 (Figure 3). The model determines these abilities for the

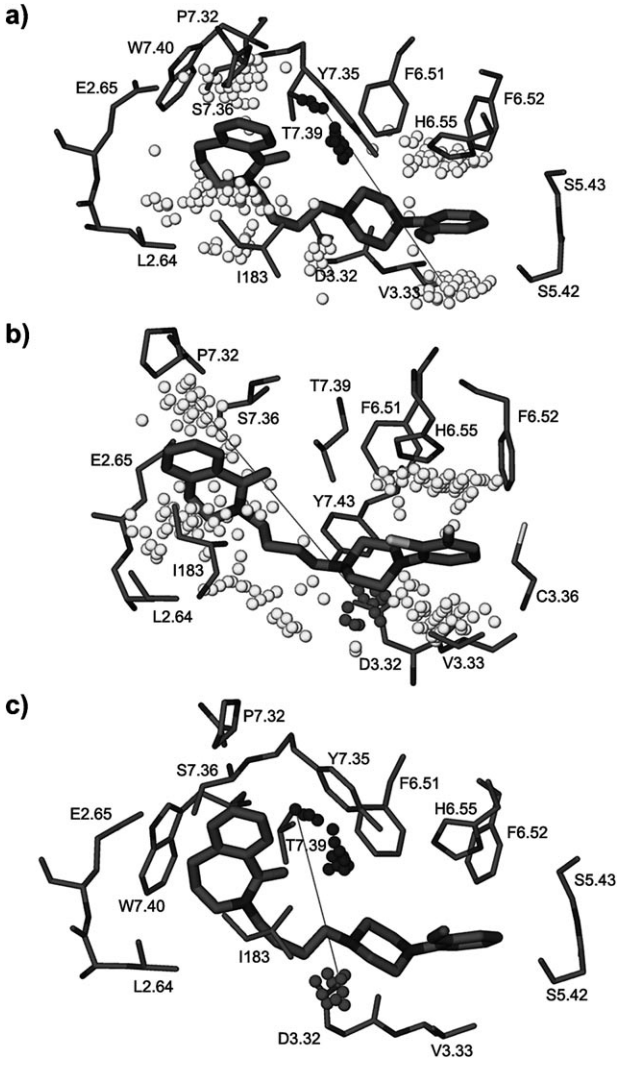

Figure 3. Complex of the D_2 receptor with compounds a) **14a**, depicting DRY–N1 variable A, b) **12f**, depicting DRY–O variable B, and c) **14a**, depicting O–N1 variable C.

compounds by identifying the distance to these hydrophobic and hydrogen bond acceptor hotspots (generated, respectively, by the aromatic moiety and benzolactam carbonyl of fragment II), with respect to other structural features present in all compounds: variable A in the DRY–N1 correlogram describes the distance between the benzolactam carbonyl and the aromatic ring (Figure 3a); variable B in the DRY–O correlogram represents the distance between the aromatic ring and the basic nitrogen (Figure 3b), and variable C in the O–N1 correlogram is the distance between the carbonyl group and the same basic nitrogen (Figure 3c). When superimposed with the receptor (see Figure 3), one can visualize how these variables together describe the aforementioned interaction between fragment II and Thr7.39, and the precise overlapping of these hotspots with atoms of the receptor binding site. It must also be noted that these variables simultaneously represent a set of structural characteristics, including linker length and type of scaffold, thus providing a complete overview of the combination of structural features that determine binding affinity for these compounds. The significance of linker length has been reported in previous SAR studies[14] which also described the interaction between the fragment II carbonyl and Thr7.39, and is further supported by the work of Ehrlich et al.[25] Mutagenesis data corroborates the hypothesis that residue 7.39 is involved in antagonist and agonist binding affinity[26–28] and substantiates the importance of Val3.33,[29] located at the opposite end of the distance represented by variable A (see Figure 3a).

With regard to the variables that have negative coefficients, variable F in the O–TIP correlogram of M1 (Figure 2a) identifies compounds with a shorter linker (three instead of four carbons), which are, therefore, unable to project fragment II into a favorable environment as mentioned previously and which, consequently, cannot establish a hydrogen bond between the carbonyl and polar residue Thr7.39 in TM7. Variable D in the N1–N1 correlogram describes the presence in fragment I of a pyridyl or pyrimidyl ring, identified by the presence at a certain distance of two groups of hydrogen bond donor (HBD) hotspots, one near the benzolactam carbonyl and the other in front of the pyridyl or pyrimidyl moiety present in fragment I of some compounds (e.g., **5c** and **5d**; Figure 4a). Inspection of the D_2 receptor complexes explains the presence of a negative coefficient, because the polar group of fragment I is located in a hydrophobic environment for these compounds, prohibiting the establishment of favorable interactions (Figure 4a). Variables with negative coefficients, labeled in Figure 2a as E, E′, and E″, are also related to fragment I and identify the presence of a *p*-methoxy substituent (e.g., compounds **5b**, **6b**, **7b**, **12b**, **14b**, and **15b**) that is consistently associated with decreased affinity for the D_2 receptor. The presence of this group is reflected in several correlograms, such as TIP–TIP (E″ variable), which links both ends of the molecular shape (Figure 4b), or N1–TIP (E and E′ variables), which identifies the unfavorable distance between the HBD hotspots proximal to the fragment II carbonyl and the protruding fragment I methoxy group.

In order to understand the negative influence of the *p*-methoxy substituent, we analyzed the D_2 receptor complexes with compounds **12a** (bearing an *o*-methoxy group) and **12b** (bearing a *p*-methoxy group) and determined that a network of polar interactions between Ser7.36, Glu2.65 and Trp7.40 (SEW network, Figure 5a) limits the extent of the binding pocket, preventing good fitting of the benzolactam ring for those compounds with a fragment I *p*-methoxy substituent (compound **12b**; Figure 5a). Consequently, the binding site does not have sufficient space to accommodate the longest ligands and, therefore, cannot establish the key hydrogen bond interaction between the carbonyl oxygen and Thr7.39 or the

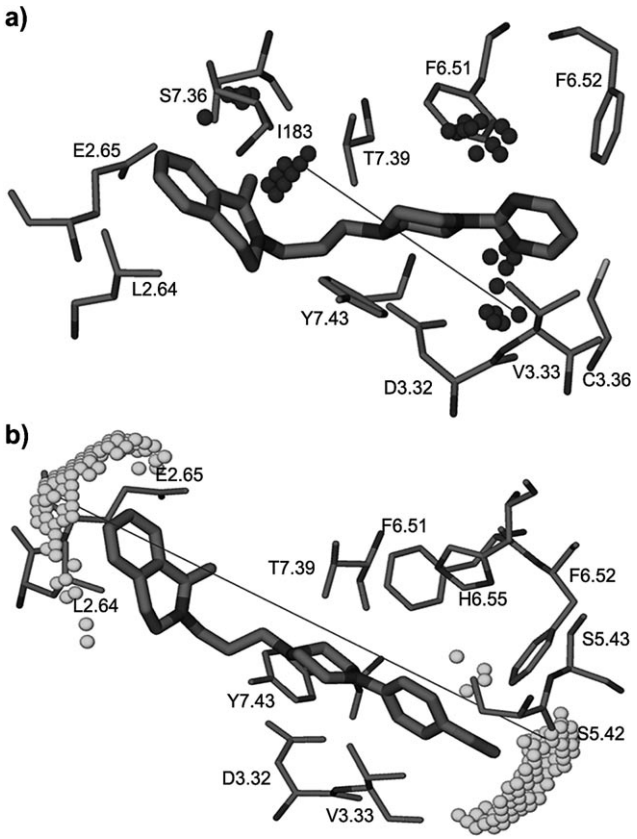

Figure 4. Complex of the D_2 receptor with a) compound **5d**, showing variable D (N1–N1 correlogram); the nitrogen heteroatoms of the pyrimidyl ring are far from other polar groups and thus unable to form interactions; b) compound **5b**, depicting variable E′′ (TIP–TIP correlogram) showing the presence of a *p*-methoxy group in fragment I.

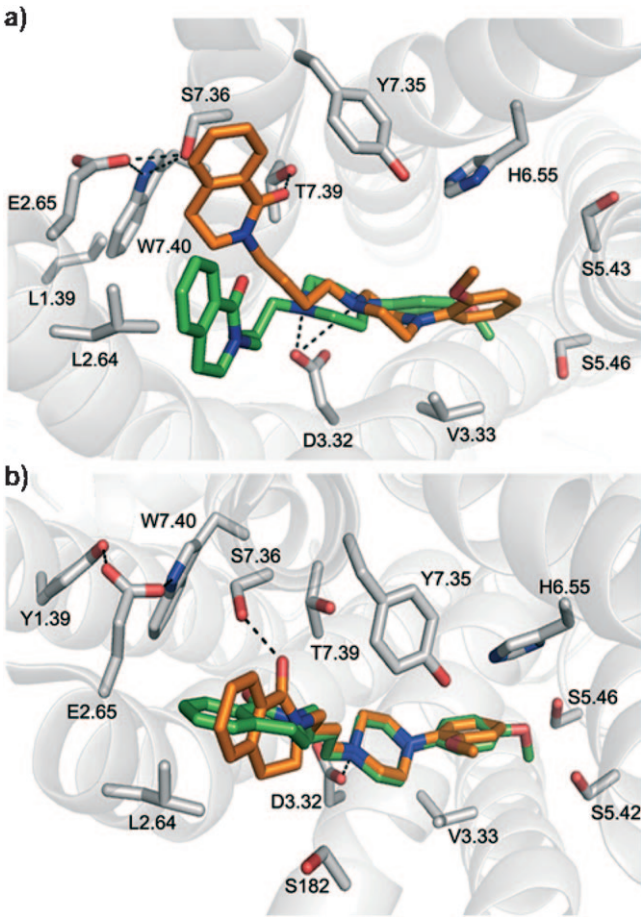

Figure 5. Complex of the a) D_2 and b) D_3 receptors with compounds **12a** (orange) and **12b** (green).

hydrophobic interactions of the benzolactam with Leu2.64 and Tyr7.35.

3D-QSAR model for D_3 receptor affinity

A similar 3D-QSAR model was built using binding affinity values for the D_3 receptor. In this case, the binding affinity values span 4.3 log units (from 4.5 to 8.8). The final PLS model (M2) was also obtained after two sequential steps of FFD variable selection, contains 279 variables, and exhibits optimum predictive ability with three LVs (Table 4). The obtained model was excellent in quality and an interpretation was attempted by analyzing the variables with the largest coefficients, represented in Figure 2b.

Unsurprisingly, variables with the highest positive coefficients (A, A′, B, and C) represent the same information found for similar variables in M1; compounds with high binding affinity are characterized by the projection of fragment II into a pocket similar to that described for the D_2 receptor, wherein fragment II is stabilized by hydrophobic residues Leu2.64 and Tyr7.35, and the carbonyl oxygen can interact with a polar residue in TM7 (Ser7.36 in this case; Figure 5b). The implication of residues Leu2.64 and Ser7.36 in ligand binding, as proposed by our models, has been corroborated by mutagenesis experiments.[25,30,31] It should be mentioned that the D_3 receptor binding site is very similar to that of the D_2 receptor, as they are nearly identical in sequence at this region. However, the Leu1.39 residue present in the D_2 receptor site is replaced in the D_3 receptor site by Tyr1.39, which interacts with Glu2.65 (Figure 5b), and thus does not exhibit the SEW interaction network described above (Figure 5a). This difference introduces two subtle changes within the binding site: first, the absence of the SEW network translates to a larger amount of space in the end of the pocket, and second, Ser7.36 is now available to create a polar interaction with the benzolactam ring of the ligand.

The interpretation of variables A, A′, B, and C in model M2 is similar to the analysis previously provided for model M1. However, it is worth mentioning that the distances between the regions represented by variables A and C are significantly longer in M2 (Figure 6) as compared with M1 (Figure 3a). In both cases, the variables describe the interactions between the benzolactam carbonyl oxygen and polar residues of TM7. In the D_2 receptor site, Thr7.39 is the main residue involved, as Ser7.36 participates in the SEW interaction. In contrast, the Ser7.36 residue in the D_3 receptor site is free to interact with the ligand, extending the area for interaction; consequently, the variables

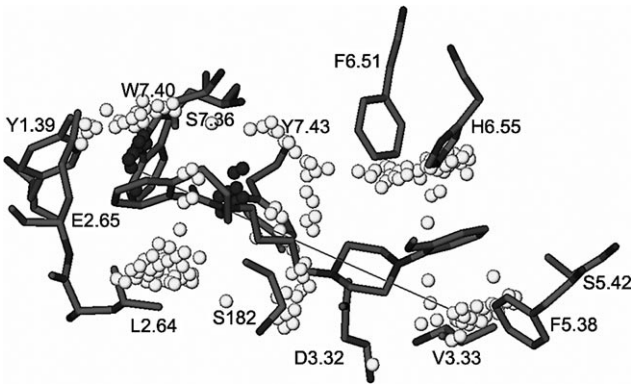

Figure 6. Complex of compound **14a** with the D_3 receptor, showing variable A from the DRY–N1 correlogram.

represent longer distances in the D_3 receptor model (Figure 3a and Figure 6).

In regard to those variables with negative coefficients in M2 (Figure 2b), variable D is identical to variable D for M1 and represents unfavorable effects on binding affinity observed for compounds in which fragment I contains a pyridyl or pyrimidyl ring. Variable F of M2, as in M1, represents an alternative and less effective position of the benzolactam ring. However, in this case the variable is part of the O–N1 correlogram, precisely describing the unfavorable location of the fragment II carbonyl oxygen in terms of its distance to the common basic nitrogen (see Figure 7). The distance represented by this variable is attributed to the short (three-carbon) linker, as well as the incorporation of scaffold D for fragment II, which appears to be more detrimental for binding affinity than in the case of the D_2 receptor.

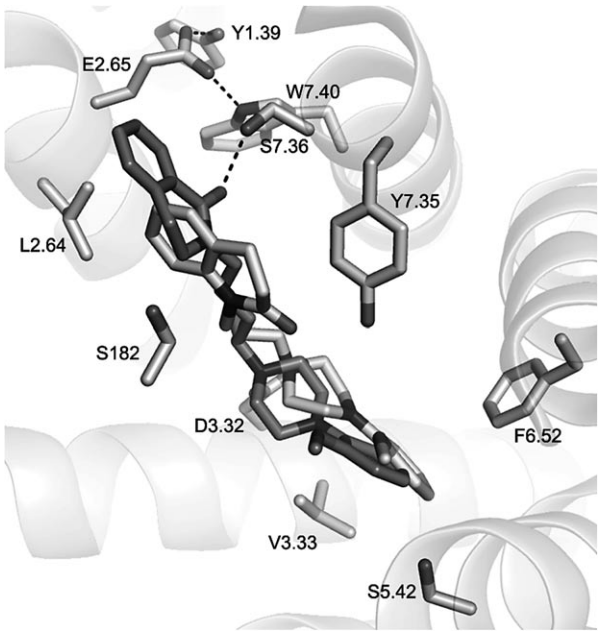

Figure 7. The D_3 receptor in complex with scaffold-A-based compound **5a** (dark gray) and scaffold-D-based compound **15a** (light gray).

Our D_3 receptor complexes were analyzed to provide further rationalization for this hypothesis. In scaffold-D-type compounds, such as compound **15a** (represented in light gray, Figure 7), the benzolactam ring is located in the binding pocket between Ser182 and Ser7.36, directing the carbonyl oxygen toward Tyr7.35 in an orientation which prevents the establishment of a hydrogen bond with Ser7.36. In contrast, the carbonyl oxygen in a compound of the isomeric form A, as in compound **5a** (represented in dark gray, Figure 7), is in the correct orientation to form this hydrogen bond, resulting in a high D_3 receptor binding affinity.

Remarkably, the M2 coefficient plot (Figure 2b) does not contain the TIP–TIP variables, labeled as E′′ in M1 (Figure 2a) and representing the detrimental effect of the *p*-methoxy substituent, although this negative effect is weaker for other variables not discussed here. In agreement with observations described in the SAR analysis, *p*-methoxy substituents produce an overall decrease in binding affinity, with the effect more intense for the D_2 receptor than for D_3 receptor. For example, *o*-methoxyphenylpiperazines **6a** and **12a** have pK_i values of 6.10 and 7.91, respectively, for the D_2 receptor and 6.68 and 8.58 for the D_3 receptor; *p*-methoxyphenylpiperazines **6b** and **12b** exhibit very low affinity for the D_2 receptor and affinities of 5.96 and 6.31, respectively, for the D_3 receptor. Our structural models of receptor D_3 in complex with compound **12a**, which has *o*-methoxy substitution, and compound **12b**, bearing a *p*-methoxy substituent, suggest a possible explanation for this effect. As shown in Figure 5b, the absence of the SEW interaction in the D_3 receptor accommodates fragment II of compound **12b** in a position where it can establish hydrophobic interactions with Leu2.64 and Tyr7.35, as well as a weak polar interaction between the carbonyl oxygen and Ser7.36.

In the SAR analysis reported above, we mentioned the effect of replacing scaffold D by scaffold E on the binding affinities for D_2 and D_3. Our 3D-QSAR models do not provide any explanation for this observation, most likely because only a few compounds in the series are of the scaffold E type, although direct analyses of the ligand–receptor complex structures may provide further insight. For the compounds in Table 1, increasing the size of the benzolactam from a six- to a seven-membered ring (scaffold A to scaffold B) produces an increase in the binding affinity, although for the isomers in Table 2, a similar change (from scaffold D to scaffold E) is associated with decreased affinity (e.g., compound **7f** to **8f**). In our models, the six-membered ring of scaffold D (e.g., compound **7f**) adopts a fairly planar conformation in both the D_2 receptor (Figure 8a) and the D_3 receptor (Figure 8b), fitting into the tight crevice formed by the SEW network, Tyr7.35, and residue Ile183 (D_2)/Ser182 (D_3) of the ECL2, where it can further establish a hydrogen bond with polar residues of TM7 (Thr7.39 and Tyr7.35 in the D_2 and D_3 receptor, respectively). In contrast, the bulkier and less planar seven-membered isolactam ring of scaffold E (e.g., **8f**) does not fit within this cleft, due to direct contacts with the SEW network and ECL2 residues. This forces fragment II into a different position (see compound **8f** in light gray in Figure 8), which is unfavorable for the formation of a hydrogen bond with TM7, and justifies the observed decrease in binding

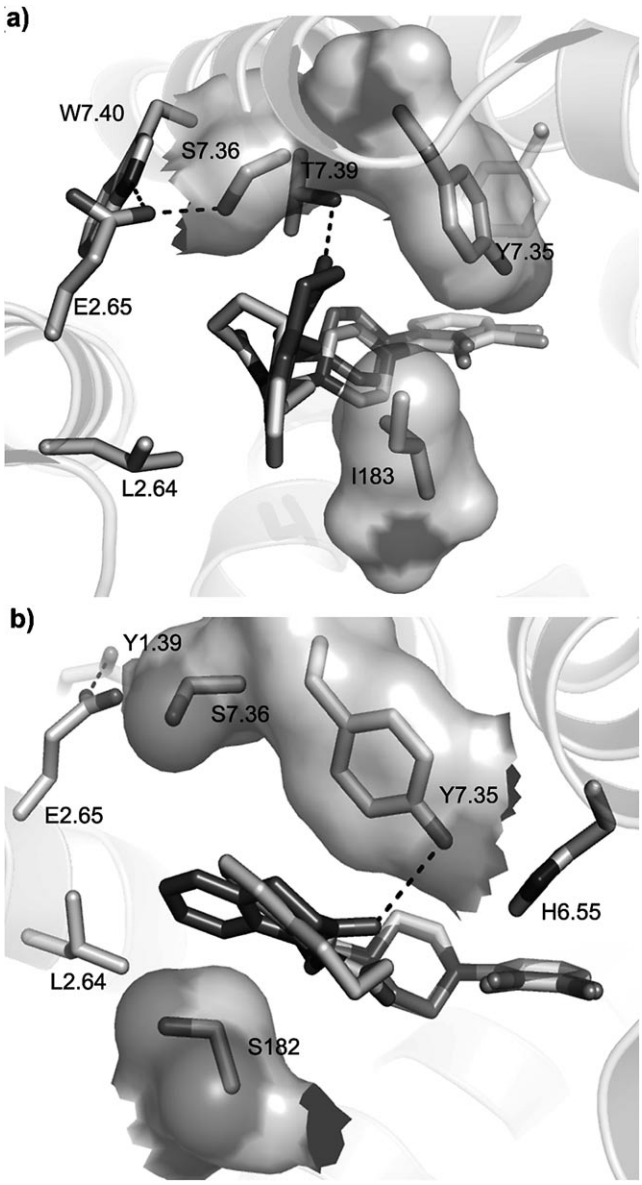

Figure 8. Complexes of compounds **7 f** (dark gray) and **8 f** (light gray) with a) D_2 and b) D_3 receptors.

affinity for D_2 and D_3. It is widely accepted that ECL2 has implications for ligand binding; direct proof was provided by the finding that mutation of Ser182 to Ile182 in the D_3 receptor affects D_3/D_2 selectivity,[25] thus confirming our models. Moreover, recent work by Newman et al.[32] demonstrated that the D_3/D_2 receptor selectivity of structurally closely related compounds (heterobiarylcarboxamides) is dependent on the ECL2.

3D-QSAR models for D_3/D_2 receptor selectivity

Models M1 and M2 exhibit notable differences, which can be conveniently summarized in a model built ad hoc to describe D_3/D_2 receptor selectivity. Toward this end, we defined a binary selectivity index, computed from the binding affinity described above only for compounds with relevant affinity for the D_3 receptor (see Experimental Section for details). This index was used to build a PLS-DA model (M3), obtaining the best results with two LVs (see Table 4). It should be noted that, for the aforementioned reasons, the training series contains only 17 compounds. This fact, coupled with the binary quality of the dependent variable, limits the quality of this model, although it is within the commonly accepted range for a reasonably good representation.

In M3, variables with positive coefficients identify features present in compounds with binding selectivity for D_3 receptor over D_2 receptor, while variables with negative coefficients represent those structural features which do not contribute to selectivity (Figure 2c). Variables with the highest positive coefficients are labeled as G in the O–N1 correlogram and H in the O–TIP correlogram. Variable G corresponds to the distance between the basic nitrogen of the piperazine ring and the carboxyl of the fragment II benzolactam. This is the same interaction described by variable C in M1 and M2, although the values for these distances are shorter (9.2–9.6 Å) for M1 and longer (12.8–13.2 Å) for M2. Variable G of M3 defines a differential structural feature, represented by the intermediate distance between the nitrogen and carbonyl regions (11.6–12.0 Å), which can be attributed to differences in D_2/D_3 receptor binding affinity. From a structural point of view, this difference can be explained by the presence of the aforementioned SEW network, in which the D_2 receptor causes Ser7.36 to become less accessible for interaction with the benzolactam carbonyl of the ligand, whereas D_3 favors this interaction. In Figure 9, the regions highlighted by variable G can be compared for the complexes of compound **14 b** with the D_2 receptor and the structure of compound **9 b** in complex with the D_3 receptor (Figure 9c). The other variable with a high positive coefficient in M3, variable H, corresponds to the distance between the basic nitrogen of the piperazine ring and the outer border of fragment II, as shown in Figure 10. Our structural models indicated that again, the SEW network might play a role in the observed binding affinity differences, as was described above for M1 (see Figure 5). For the D_2 receptor, the SEW network hinder access to the distal region of the pocket; therefore, longer compounds, such as those with a *p*-methoxy substituent, bind more tightly to the D_3 receptor, which does not contain this network.

The negative coefficients of M3, specifically, variable I in the N1–N1 correlogram and J in the N1–TIP correlogram (Figure 2c) again reflect the effect of the total compound length and of the *p*-methoxy substituent. In both cases, the presence of a short distance between the common region defined by the benzolactam carbonyl and other distinctive regions, namely the hydrogen bond acceptor regions present in compounds with pyrimidyl or pyridyl groups (variable I) or the outer border of fragment I (variable J), is unfavorable for selectivity toward the D_2 receptor.

Conclusions

We synthesized a series of 37 benzolactam compounds and determined their binding affinities for the D_2 and D_3 receptors. This series has been used to explore the effects of diverse

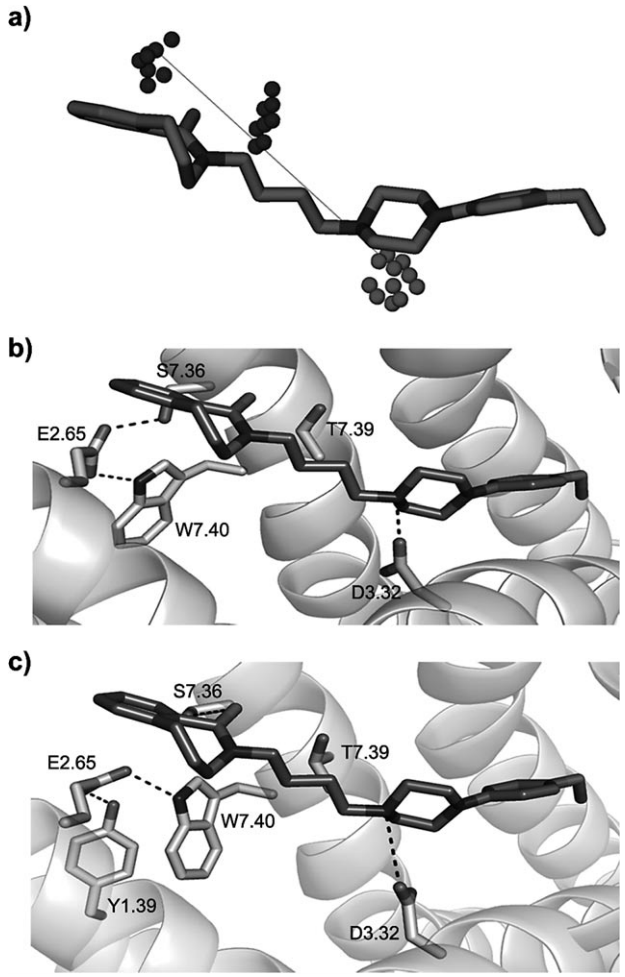

Figure 9. a) Variable G as presented for compound **14b**. Compound **14b** in complex with b) D_2 and c) D_3 receptors.

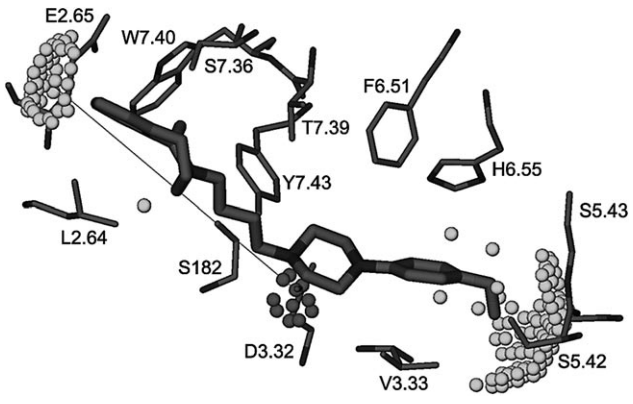

Figure 10. Complex of compound **14b** with the D_3 receptor, showing variable H from the O–TIP correlogram.

structural features on binding affinities for dopamine receptors. In spite of the high level of homology present in the binding sites of these receptors, the findings extracted from 3D-QSAR analyses enabled us to identify structural differences which may explain the experimentally observed binding affinities for the series, which were further confirmed via analysis of the ligand–receptor complex structures.

With respect to the overall binding affinity of the compounds, we have shown the importance of positioning the fragment II benzolactam moiety in a favorable manner for establishing direct interactions between the carbonyl oxygen of the benzolactam ring and the polar residues of TM7 (Ser7.36 in the D_2 receptor and Thr7.39 in the D_3 receptor). For scaffold-A- or B-type compounds with a butyl linker, this interaction is also stabilized by hydrophobic interactions between the benzolactam ring and residues Leu2.64 and Tyr7.35. Furthermore, the structural models of the complexes highlight the important influence of fragment I substituents on binding affinity; compounds with a pyridyl or pyrimidyl moiety have a lower binding affinity for both the D_2 and D_3 receptors, as do those containing a *p*-methoxy substituent.

In terms of D_3 receptor selectivity, our 3D-QSAR and structural models concur, indicating that the factors that most influence preference for this receptor are overall compound length and *p*-methoxy group substitutions on the aryl moiety. Analysis of the complexes suggested that an interaction network present only in the D_2 receptor (the SEW network) prevents longer compounds from establishing the number of favorable interactions possible in the D_3 receptor, which lacks this network. This finding justifies our earlier observations and can also be exploited for the purpose of designing novel D_3 selective compounds, introducing substituents to the benzolactam moiety that clash with members of the SEW network or designing compounds with bulkier substituents at the *p*-position of the aryl moiety, for example.

In summary, analyses of the effects of diverse structural features on binding affinities for compounds of this series suggest potentially successful approaches for the design of D_3 selective compounds: 1) using a benzolactam moiety with a seven-membered ring (scaffold B) in fragment II, 2) including a 4-carbon linker between fragment II and the piperazine ring, and 3) introducing a *p*-methoxyaryl substituent to fragment I. The results presented here also demonstrate how 3D-QSAR approaches, used in combination with SBDD, constitute a powerful tool for determination of the molecular mechanisms that determine binding affinity for members of this series of compounds toward different receptors.

Experimental Section

Chemistry

All chemicals were purchased from commercial sources (e.g., Sigma–Aldrich Chemical Co.) where available and used without further purification. When necessary, solvents were purified by distillation over an appropriate drying agent under argon atmosphere and used immediately. Melting points were determined with a Kofler hot stage instrument or a Gallenkamp capillary melting point apparatus and are uncorrected. IR spectra were recorded with a PerkinElmer 1600 FTIR spectrophotometer; the main bands are given in cm^{-1}. NMR spectra were recorded on a Bruker WM AMX (300 MHz for ^1H NMR and 75.5 MHz for ^{13}C NMR); chemical shifts (δ) were recorded in ppm downfield from $(CH_3)_4Si$ as an in-

ternal reference; approximate coupling constants (*J*) are given in Hz. All observed signals were consistent with the proposed structures. Mass spectra were collected using a Kratos MS-50 or a Varian Mat-711 mass spectrometer by chemical ionization (CI) or electron impact (EI) methods. Flash column chromatography was performed using Kieselgel 60 (60–200 mesh, E. Merck AG, Darmstadt, Germany). Reactions were monitored by thin-layer chromatography (TLC) on Merck 60 GF_{254} chromatogram sheets using iodine vapor and/or UV light for detection. Unless otherwise noted, each of the purified compounds was isolated as a single spot. Elemental combustion analyses were performed using a PerkinElmer 240B apparatus. The purities of all compounds tested were >95% as determined by elemental analysis. Hydrochlorides were prepared by dropwise addition, with cooling, of a saturated solution of HCl gas in anhydrous Et_2O to a solution of the amine in anhydrous Et_2O or absolute MeOH/Et_2O.

General procedure for the preparation of benzolactams by Schmidt reaction. NaN_3 (2.46 g, 37.84 mmol) was added portionwise to an ice-cooled solution of the benzocycloalkanone (18.92 mmol) in concentrated HCl (50 mL). The resulting mixture was stirred at 0 °C for 30 min, then warmed to room temperature while stirring overnight. Next, the reaction mixture was poured into ice water (200 mL), basified to pH 9 with K_2CO_3, and extracted with CH_2Cl_2. The organic layers were combined, dried over anhydrous Na_2SO_4 and concentrated under reduced pressure to give the crude lactam. Purification by silica gel chromatography (EtOAc/hexanes 2:1 → EtOAc) provided the desired benzolactam.

3,4-Dihydroisoquinolin-1(2*H*)-one (2a). Light yellow needles, 75% yield; mp: 98–100 °C. Spectroscopic data agree with published values.[33]

3,4-Dihydroquinolin-2(1*H*)-one (3a). White solid, 10% yield; mp: 165–166 °C. Spectroscopic data agree with published values.[33]

2,3,4,5-Tetrahydrobenzo[*c*]azepin-1-one (2b). White solid, 87% yield; mp: 102–103 °C. Spectroscopic data agree with published values.[18]

1,3,4,5-Tetrahydrobenzo[*b*]azepin-2-one (3b). Off-white solid, 7% yield; mp: 141–142 °C. Spectroscopic data agree with published values.[18]

General procedure for the preparation of benzolactams by Beckmann reaction. A solution of $NH_2OH{\cdot}HCl$ (1.03 g, 14.77 mmol) in H_2O (2 mL) was added to a solution of the benzocycloalkanone (11.36 mmol) dissolved in MeOH (20 mL). The resulting mixture was cooled to −10 °C in a salt–ice bath, and a solution of 4 N NaOH (4.32 mL, 17.46 mmol) was added dropwise. After 5 min, the cold bath was removed and the reaction was kept at room temperature for 2 h. The reaction was quenched by adding 50 mL H_2O. The resulting white solid formed was filtered to provide the desired oxime. Further extraction of the filtrate with EtOAc increased the yield of oxime.

The oxime (5.1 mmol) and toluenesulfonyl chloride (1 g, 5.6 mmol) were dissolved in acetone (30 mL) while stirring. The resulting mixture was cooled to −10 °C in a salt-ice bath, and a 4 N solution of NaOH was added dropwise. A white precipitated formed immediately. The reaction mixture was stirred for a further 5 min at low temperature, then for 1 h at room temperature. At this point, the reaction was quenched by adding 200 mL of ice water. The aqueous phase was extracted with EtOAc, the combined organic layers dried over Na_2SO_4, and the solvent evaporated under reduced pressure to give the crude *O*-toluenesulfonyloxime as a white solid.

$AlCl_3$ (4.98 mmol, 0.66 g) was added slowly to a solution of the *O*-toluenesulfonyloxime (1.7 mmol), in CH_2Cl_2 (15 mL) at −40 °C. After 10 min, the reaction was warmed to room temperature and continued to stir for an additional 1 h. The reaction was then quenched by careful addition of H_2O (50 mL) and extracted with CH_2Cl_2 (4× 20 mL). The extract was dried over Na_2SO_4 and evaporated under reduced pressure. Lactams were isolated by chromatography on a silica gel column (EtOAc/hexanes 2:3) as white solids in the following yields:

3,4-Dihydroisoquinolin-1(2*H*)-one (**2a**): Yield 5%.

3,4-Dihydroquinolin-2(1*H*)-one (**3a**): Yield 60%.

2,3,4,5-Tetrahydrobenzo[*c*]azepin-1-one (**2b**): Yield 5%.

1,3,4,5-Tetrahydrobenzo[*b*]azepin-2-one (**3b**): Yield 85%.

Method A: preparation of substituted *N*-arylpiperazinylpropylbenzolactams

General procedure for the preparation of *N*-propylpiperazines 4a–f. 1-Bromo-3-chloropropane (1.54 mL, 15.6 mmol) was added dropwise to a stirred solution of the N-substituted piperazine (15.6 mmol) and 6 M $NaOH_{(aq)}$ (2.7 mL, 16.2 mmol) in acetone (40 mL). The reaction mixture was stirred for 48 h at room temperature. The solvent was then evaporated under reduced pressure and the residue re-dissolved in H_2O. This solution was extracted with CH_2Cl_2, the organic layers dried over Na_2SO_4, and the solvent concentrated. The residue was purified by chromatography on a silica gel column (eluent: EtOAc/hexanes) to obtain the title compounds **4a**–**f**.

1-(3-Chloropropyl)-4-(2-methoxyphenyl)piperazine (4a). White solid, 71% yield; mp: 55–56 °C. Spectroscopic data agree with published values.[34,35]

1-(3-Chloropropyl)-4-(4-methoxyphenyl)piperazine (4b). Off-white solid, 72% yield; mp: 74–75 °C. Spectroscopic data agree with published values.[36]

1-(3-Chloropropyl)-4-(2-pyridyl)piperazine (4c). Very dense, light yellow oil, 61% yield. Spectroscopic data agree with published values.[36]

1-(3-Chloropropyl)-4-(2-pyrimidyl)piperazine (4d). For this reaction, 3 equiv $NaOH_{(aq)}$ were used due to the use of the *N*-(2-*p*yrimidyl)piperazine as a dihydrochloride salt. Yellow solid, 68% yield; mp: 59–61 °C. ^{1}H NMR ($CDCl_3$): δ = 8.27 (d, 2H, J = 4.7), 6.44 (t, 2H, J = 4.7), 3.79 (t, 4H, J = 5.1), 3.60 (t, 2H, J = 6.5), 2.51–2.45 (m, 6H), 1.95 (q, 2H, J = 6.8).

1-(2,3-Dichlorophenyl)-4-(chloropropyl)piperazine (4e). For this reaction, 2 equiv $NaOH_{(aq)}$ were used due to the use of *N*-(2,3-dichlorophenyl)piperazine as a monohydrochloride salt. White solid, 80% yield; mp: 74–75 °C. ^{1}H NMR ($CDCl_3$): δ = 7.15–7.13 (m, 2H), 6.96–6.93 (m, 1H), 3.62 (t, 2H, J = 6.5), 3.06 (br d, 4H, J = 4.1), 2.63–2.54 (m, 6H), 2.03–1.94 (m, 2H).

1-(3-Chloropropyl)-4-(3-trifluoromethyl)piperazine (4f). Very dense, brown oil, 63% yield. Spectroscopic data agree with published values.[36]

General Procedure for Preparation of the *N*-[3-(4-Arylpiperazin-1-yl)propyl]benzolactams 5–8. 60% NaH (98 mg, 2,45 mmol) was slowly added to a stirred solution of benzolactam **2a**–**b** or **3a**–**b** (1.36 mmol) in anhydrous benzene (3 mL) under argon atmosphere. The resulting suspension was held at reflux for 1 h and cooled to room temperature, then a solution of the substituted *N*-

(3-chloropropyl)piperazine (**4a–f**; 2.72 mmol) in 5 mL of benzene was added dropwise. The mixture was held at reflux at 90 °C for 72 h, then the solvent was evaporated under reduced pressure. The crude oil was purified by column chromatography (eluent: EtOAc/hexanes, proportions depending on the compound); to afford the title compounds **5**–**8** as dense oils, some of which cases crystallized.

3,4-Dihydro-*N*-[3-(4-(2-methoxyphenyl)piperazin-1-yl)propyl]isoquinolin-1(2*H*)-one (5a). Viscous yellow liquid, 70% yield. ^{1}H NMR ($CDCl_3$): δ = 8.07 (dd, 1H, J = 7.6, 1.3), 7.43–7.31 (m, 2H), 7.17 (dd, 1H, J = 7.8, 1.2), 7.02–6.84 (m, 4H), 3.85 (s, 3H), 3.66–3.56 (m, 4H), 3.10 (brs, 4H), 2.99 (t, 2H, J = 6.6), 2.67 (brs, 4H), 2.53–2.48 (m, 2H), 1.89 (q, 2H, J = 7.3); ^{13}C NMR ($CDCl_3$): δ = 164.8, 152.7, 142.0, 138.4, 131.9, 130.0, 128.6, 127.4, 127.2, 123.3, 121.4, 118.6, 111.6, 56.3, 55.7, 53.9, 51.0, 46.7, 46.2, 28.6, 25.6; IR (film): 2938, 1646, 1499, 1400, 1240; MS (EI) m/z 379 ([M]$^+$, 8), 364 (29), 230 (32), 217 (79), 186 (100), 160 (43); *Chlorhydrate*: white solid; mp: 221–222 °C; Anal. calcd for $C_{23}H_{29}N_3O_2$·HCl·0.3 CH_3OH·0.7 H_2O: C 58.96, H 7.14, N 8.85%, found: C 58.95, H 7.15, N 8.88%.

3,4-Dihydro-*N*-[3-(4-(4-methoxyphenyl)piperazin-1-yl)propyl]isoquinolin-1(2*H*)-one (5b). White solid, 75% yield; mp: 76–77 °C (cyclohexane). ^{1}H NMR ($CDCl_3$): δ = 7.54 (dd, 1H, J = 7.5, 1.2), 7.43–7.30 (m, 2H), 7.16 (d, 1H, J = 7.4), 6.91–6.81 (m, 4H), 3.75 (s, 3H), 3.65–3.56 (m, 2H), 3.09 (t, 4H, J = 4.8), 2.99 (t, 2H, J = 6.6), 2.67–2.65 (t, 4H, J = 4.9), 2.51–2.46 (m, 2H), 1.88 (q, 2H, J = 7.3); ^{13}C NMR ($CDCl_3$): δ = 164.8, 154.2, 146.1, 138.4, 131.9, 130.01, 128.6, 127.4, 127.2, 118.5, 114.8, 56.2, 56.0, 53.8, 51.0, 46.8, 46.2, 28.6, 25.6; IR (KBr): 2943, 2823, 1708, 1643, 1512, 1311; MS (EI) m/z 379 ([M]$^+$, 97), 364 (78), 217 (100), 205 (43), 186 (69), 160 (43); *Chlorhydrate*: white solid; mp: 216–219 °C (dec.); Anal. calcd for $C_{23}H_{29}N_3O_2$·2 HCl·0.15 CH_3OH·0.75 H_2O: C 59.07, H 7.09, N 8.93%, found: C 58.95, H 6.93, N 8.93%.

3,4-Dihydro-*N*-[3-(4-(2-pyridyl)piperazin-1-yl)propyl]isoquinolin-1(2*H*)-one (5c). White solid, 54% yield; mp: 91–92 °C (cyclohexane). ^{1}H NMR ($CDCl_3$): δ = 8.19–8.17 (m, 1H), 8.08 (d, 1H, J = 7.5), 7.49–7.31 (m, 3H), 7.17 (d, 1H, J = 7.4), 6.65–6.59 (m, 2H), 3.66–3.48 (m, 8H), 2.99 (t, 2H, J = 6.6), 2.57 (t, 4H, J = 5.1), 2.50–2.45 (m, 2H), 1.89 (q, 2H, J = 7.3); ^{13}C NMR ($CDCl_3$): δ = 164.5, 160.0, 148.3, 138.5, 137.8, 131.9, 130.0, 128.6, 127.4, 127.2, 113.7, 107.5, 56.3, 53.5, 46.8, 46.3, 45.6, 28.7, 25.6; IR (KBr): 2932, 1642, 1596, 1482, 1436, 1312, 1246; MS (EI) m/z 350 ([M]$^+$, 8.5), 256 (44), 207 (84), 188 (91), 160 (46), 107 (100); *Chlorhydrate*: white solid; mp: 237–238 °C; Anal. calcd for $C_{21}H_{26}N_4O$·2 HCl·0.4 CH_3OH·0.6 H_2O: C 57.50, H 6.94, N 12.53%, found: C 57.50, H 6.94, N 12.53%.

3,4-Dihydro-*N*-[3-(4-(2-pyrimidyl)piperazin-1-yl)propyl]isoquinolin-1(2*H*)-one (5d). Yellow oil, 21% yield. ^{1}H NMR ($CDCl_3$): δ = 8.27 (d, 2H, J = 4.7), 7.63 (dd, 1H, J = 7.6, 1.3), 7.41–7.34 (m, 2H), 7.15 (d, 1H, J = 7.4), 6.45 (t, 1H, J = 4.7), 3.84–3.81 (m, 4H), 3.64–3.55 (m, 4H), 2.97 (t, 2H, J = 6.6), 2.54–2.45 (m, 6H), 1.89 (q, 2H, J = 7.3); ^{13}C NMR ($CDCl_3$): δ = 164.8, 162.0, 158.1, 138.3, 131.9, 129.9, 128.5, 127.4, 127.2, 110.2, 56.3, 53.5, 46.70, 46.2, 44.0, 28.6, 25.5; IR (film): 2940, 2852, 1646, 1600, 1550, 1500; MS (EI) m/z 351 ([M]$^+$, 4), 243 (47), 186 (100), 148 (67), 122 (72); *Chlorhydrate*: light yellow solid; mp: 216–217 °C; Anal. calcd for $C_{20}H_{25}N_5O$·2 HCl·1.4 H_2O: C 53.43, H 6.68, N 15.58%, found: C 53.33, H 6.71, N 15.74%.

3,4-Dihydro-*N*-[3-(4-(3-trifluoromethylphenyl)piperazin-1-yl)propyl]isoquinolin-1(2*H*)-one (5e). Yellow oil, 53% yield. ^{1}H NMR ($CDCl_3$): δ = 8.08 (dd, 1H, J = 7.6, 1.3), 7.43–7.31 (m, 3H), 7.17 (d, 1H, J = 7.4), 7.10–7.03 (m, 3H), 3.66–3.57 (m, 4H), 3.24 (t, 4H, J = 5.03), 2.99 (t, 2H, J = 6.6), 2.66–2.58 (m, 4H), 2.52–2.47 (m, 2H), 1.89 (q, 2H, J = 7.3); ^{13}C NMR ($CDCl_3$): δ = 164.8, 151.8, 138.4, 132.0, 131.9, 130.5, 129.9, 128.5, 127.3, 127.2, 126.0, 119.0, 116.2, 112.5, 56.1, 53.4, 49.0, 46.8, 46.2, 28.6, 25.6; IR (film): 2943, 2824, 1646, 1488, 1451, 1314, 1238; MS (EI) m/z 417 ([M]$^+$, 2), 243 (42), 217 (70), 186 (100), 160 (36), 118 (34); *Chlorhydrate*: light orange solid; mp: 142–145 °C; Anal. calcd for $C_{23}H_{26}F_3N_3O$·HCl·1.5 H_2O: C 57.44, H 6.29, N 8.74%, found: C 57.39, H 6.41, N 8.88%.

3,4-Dihydro-*N*-[3-(4-(2,3-dichlorophenyl)piperazin-1-yl)propyl]-isoquinolin-1(2*H*)-one (5f). Yellow solid, 86% yield; mp: 92–94 °C. ^{1}H NMR ($CDCl_3$): δ = 8.07 (dd, 1H, J = 7.6, 1.1), 7.43–7.31 (m, 2H), 7.21–7.09 (m, 3H), 6.94 (dd, 1H, J = 6.4, 3.3), 3.66–3.57 (m, 4H) 3.08 (brs, 4H), 2.99 (t, 2H, J = 6.6), 2.68 (brs, 4H), 2.56–2.51 (m, 2H), 1.95–1.85 (q, 2H, J = 7.3, 1.9); ^{13}C NMR ($CDCl_3$): δ = 164.8, 151.6, 138.3, 134.4, 131.9, 129.5, 128.6, 127.8, 127.4, 127.2, 126.2, 124.9, 119.0, 56.2, 53.7, 51.7, 46.7, 46.2, 28.6, 25.5; IR (KBr): 2941, 2821, 1646, 1575, 1451; MS (EI) m/z 417 ([M]$^+$, 0.67), 382 (6), 243 (56), 217 (68), 186 (100), 160 (38), 118 (35); *Chlorhydrate*: white solid; mp: 232–236 °C (2-propanol); Anal. calcd for $C_{22}H_{25}Cl_2N_3O$·HCl: N 9.24, C 58.09, H 5.76%, found: N 9.31, C 58.01, H 6.07%.

2,3,4,5-Tetrahydro-*N*-[3-(4-(2-methoxyphenyl)piperazin-1-yl)propyl]benzo[*c*]azepin-1-one (6a). White solid, 26% yield; mp: 80–82 °C (cyclohexane). ^{1}H NMR ($CDCl_3$): δ = 7.66 (d, 1H, J = 7.1), 7.38–7.29 (m, 2H), 7.14–7.11 (m, 1H), 7.02–6.93 (m, 3H), 6.92–6.85 (m, 1H), 3.86 (s, 3H), 3.63 (t, 2H, J = 7.4), 3.23 (t, 2H, J = 6.4), 3.10 (brs, 4H), 2.79 (t, 2H, J = 7.1), 2.69 (brs, 4H), 2.52 (t, 2H, J = 7.5), 2.03 (q, 2H, J = 6.8), 1.92 (q, 2H, J = 7.5); ^{13}C NMR ($CDCl_3$): δ = 171.0, 153.0, 142.0, 138.0, 137.0, 131.1, 128.9, 128.5, 127.3, 123.30, 121.4, 118.6, 111.6, 56.4, 55.7, 53.9, 51.1, 46.9, 46.2, 30.7 30.4, 26.8; IR (KBr): 2941, 2819, 1708, 1632, 1499, 1454, 1372, 1239; MS (EI) m/z 378 ([M]$^+$, 15) 231 (60), 202 (70), 134 (62), 120 (100), 91 (69); *Chlorhydrate*: white solid; mp: 148–149 °C; Anal. calcd for $C_{24}H_{31}N_3O_2$·2 HCl·0.5 H_2O: N 8.84, H 7.21, C 60.63%, found: C 60.90, H 7.48, N 8.77%.

2,3,4,5-Tetrahydro-*N*-[3-(4-(4-metoxyphenyl)piperazin-1-yl)propyl]benzo[*c*]azepin-1-one (6b). White solid, 41% yield; mp: 100–101 °C (cyclohexane). ^{1}H NMR ($CDCl_3$): δ = 7.66 (d, 1H, J = 7.1), 7.36–7.28 (m, 2H), 7.13 (d, 1H, J = 7.05), 6.91 (d, 2H, J = 8.90), 6.84 (d, 2H), 3.77 (s, 3H), 3.63 (t, 2H, J = 7.3), 3.23 (t, 2H, J = 6.3), 3.13–3.10 (m, 4H), 2.79 (t, 2H, J = 7.0), 2.67–2.65 (m, 4H), 2.54–2.49 (m, 2H), 2.04 (q, 2H, J = 6.7), 1.92 (q, 2H, J = 7.4); ^{13}C NMR ($CDCl_3$): δ = 172.0, 154.1, 146.0, 138.0, 137.6, 131.1, 128.9, 128.6, 127.4, 118.6 (2C), 114.8 (2C), 56.3, 56.0, 53.8, 51.0, 46.9, 46.2, 30.7, 30.3, 26.7; IR (KBr): 2943, 1750, 1700, 1635, 1516; MS (EI) m/z 393 ([M]$^+$, 15), 378 (19) 231 (87), 202 (100), 162 (43), 135 (51), 120 (50); *Chlorhydrate*: light yellow solid; mp: 234–236 °C; Anal. calcd for $C_{24}H_{31}N_3O_2$·HCl·0.1 CH_3OH·0.15 H_2O: C 66.4, H 7.56, N 9.64%, found: C 66.37, H 7.61, N 9.64%.

2,3,4,5-Tetrahydro-*N*-[3-(4-(2-pyridyl)piperazin-1-yl)propyl]benzo[*c*]azepin-1-one (6c). White solid, 44% yield; mp: 104–105 °C (cyclohexane). ^{1}H NMR ($CDCl_3$): δ = 8.19 (dd, 1H, J = 5.1, 1.6), 7.66 (dd, 1H, J = 7.2, 1.7), 7.51–7.29 (m, 3H), 7.13 (d, 1H, J = 5.8), 6.66–6.60 (m, 2H), 3.64 (t, 2H, J = 7.4), 3.58 (brs, 4H), 3.24 (t, 2H, J = 6.4), 2.79 (t, 2H, J = 7.1), 2.64 (brs, 4H), 2.52 (t, 2H, J = 7.2), 2.09–2.02 (m, 2H), 2.02–1.91 (m, 2H); ^{13}C NMR ($CDCl_3$): δ = 171.5, 159.9, 148.3, 137.9, 137.6, 136.8, 131.1, 128.9, 128.6, 127.4, 113.8, 107.5, 56.4, 53.4, 46.9, 46.1, 45.3, 30.7, 30.3, 26.6; IR (KBr): 2942, 1750, 1635, 1615; MS (EI) m/z 364 ([M]$^+$, 0.14), 258 (100), 243 (43), 227 (43), 165 (35); *Chlorhydrate*: off-white solid; mp: 233–234 °C (EtOAc); Anal. calcd for $C_{22}H_{28}N_4O$·2 HCl·H_2O: N 12.3, C 58.02, H 7.08%, found: N 12.29, C 58.14, H 7.24%.

2,3,4,5-Tetrahydro-*N*-[3-(4-(2-pyrimidyl)piperazin-1-yl)propyl]-benzo[*c*]azepin-1-one (6d). White solid, 27% yield; mp: 112–

113 °C (cyclohexane). ^{1}H NMR ($CDCl_3$): δ = 8.29 (d, 2H, J = 4.7), 7.65 (dd, 1H, J = 7.2, 1.7), 7.27–7.38 (m, 2H), 7.12 (d, 1H, J = 7.5), 6.47 (t, 1H, J = 4.7), 3.85–3.83 (br m, 4H), 3.63 (t, 2H, J = 7.4), 3.22 (t, 2H, J = 6.4), 2.78 (t, 2H, J = 7.1), 2.48–2.45 (m, 6H), 2.04 (q, 2H, J = 6.7), 1.90 (q, 2H, J = 7.4); ^{13}C NMR ($CDCl_3$): δ = 171.5, 162.0, 158.1, 137.6, 136.8, 131.1, 128.9, 128.6, 127.4, 110.2, 56.5, 53.6, 46.9, 46.2, 44.1, 30.7, 30.3, 26.8; IR (KBr): 2926, 1711, 1627, 1583, 1445, 1360; MS (EI) m/z 365 ([M]$^+$, 5), 202 (82), 163 (12), 58 (100); *Chlorhydrate*: white solid; mp: 154–155 °C (EtOAc); Anal. calcd for $C_{21}H_{27}N_5O{\cdot}2HCl{\cdot}0.4H_2O$: N 15.72, C 56.6, H 6.76%, found: N 15.76, C 56.85, H 7.03%.

2,3,4,5-Tetrahydro-*N*-[3-(4-(3-trifluoromethylphenyl)piperazin-1-yl)propyl]benzo[*c*]azepin-1-one (6e). Yellow–orange oil, 48% yield. ^{1}H NMR ($CDCl_3$): δ = 7.66 (dd, 1H, J = 7.2, 1.7), 7.39–7.29 (m, 3H), 7.14–7.05 (m, 4H), 3.63 (t, 2H, J = 7.4), 3.27–3.21 (m, 6H), 2.79 (t, 2H, J = 7.1), 2.64 (t, 4H, J = 5.0), 2.53–2.48 (m, 2H), 2.08–1.99 (m, 2H), 1.96–1.86 (m, 2H); ^{13}C NMR ($CDCl_3$): δ = 171.5, 151.8, 137.6, 136.7, 131.1, 129.9, 128.9, 128.6, 127.4, 119.1, 117.5, 117.0, 113.0, 112.5, 56.2, 53.4, 49.0, 46.9, 46.2, 30.6, 30.3, 26.7; IR (film): 2943, 2823, 1637, 1452, 1365; MS (EI) m/z 431 ([M]$^+$, 3), 257 (27), 243 (36), 231 (82), 202 (100), 188 (31); *Chlorhydrate*: light orange solid; mp: 180–183 °C; Anal. calcd for: ($C_{24}H_{28}F_3N_3O{\cdot}HCl{\cdot}1.3H_2O$): N 8.55, C 58.66, H 6.48, found: N 8.69, C 58.56, H 6.46.

2,3,4,5-Tetrahydro-*N*-[3-(4-(2,3-dichlorophenyl)piperazin-1-yl)-propyl]benzo[*c*]azepin-1-one (6f). Brown oil, 80% yield. ^{1}H NMR ($CDCl_3$): δ = 7.66 (d, 1H, J = 7.0), 7.36–7.31 (m, 2H), 7.15–7.12 (m, 3H), 6.95 (dd, 1H, J = 6.4, 3.2), 3.64 (t, 2H, J = 7.4), 3.23 (t, 2H, J = 6.4) 3.09 (br s, 4H), 2.79 (t, 2H, J = 7.1), 2.70 (br s, 4H), 2.58–2.53 (m, 2H), 2.09–2.00 (m, 2H), 1.97–1.87 (m, 2H); ^{13}C NMR ($CDCl_3$): δ = 171.5, 151.5, 137.6, 136.6, 134.5, 131.1, 128.9, 128.7, 128.6, 127.8, 127.4, 125.0, 119.0, 56.2, 53.6, 51.5, 46.9, 46.1, 30.7, 30.3, 26.5; IR (film): 2942, 2819, 1636, 1575; MS (EI) m/z 431 ([M]$^+$, 0.36), 396 (8), 231 (75), 202 (100), 174 (31); *Chlorhydrate*: light brown solid; mp: 142–145 °C; Anal. calcd for $C_{23}H_{27}Cl_2N_3O{\cdot}HCl{\cdot}1.25H_2O$: N 8.55, C 56.22, H 6.26%, found: N 8.51, C 56.06, H 6.04%.

3,4-Dihydro-1-[3-(4-(2-methoxyphenyl)piperazin-1-yl)propyl]quinolin-2(1*H*)-one (7a). Light yellow oil, 73% yield; *Chlorhydrate*: off-white solid; mp: 182–183 °C. Spectroscopic data agree with published values.[37]

3,4-Dihydro-1-[3-(4-(4-methoxyphenyl)piperazin-1-yl)propyl]quinolin-2(1*H*)-one (7b). White solid, 71% yield; mp: 98–99 °C (cyclohexane). ^{1}H NMR ($CDCl_3$): δ = 7.23–7.09 (m, 3H), 7.02–6.97 (m, 1H), 6.92–6.82 (m, 4H), 4.01 (t, 2H, J = 7.5), 3.77 (s, 3H), 3.10 (t, 4H, J = 4.9), 2.92–2.87 (m, 2H), 2.67–2.60 (m, 6H), 2.48 (t, 2H, J = 7.2), 1.88 (q, 2H, J = 7.3); ^{13}C NMR ($CDCl_3$): δ = 170.6, 155.0, 146.1, 140.0, 128.4, 127.8, 126.9, 123.1, 118.5, 115.3, 114.8, 56.1, 56.0, 53.8, 51.0, 40.9, 32.3, 26.0, 25.1; IR (KBr): 2931, 2815, 1662, 1599, 1511, 1461, 1380; MS (EI), m/z 379 ([M]$^+$, 44), 205 (100), 188 (56); Anal. calcd for $C_{23}H_{29}N_3O_2{\cdot}1.4H_2O$: C 68.26, H 7.92, N 10.38%, found: C 67.94, H 7.64, N 10.69%.

3,4-Dihydro-1-[3-(4-(2-pyridyl)piperazin-1-yl)propyl]quinolin-2(1*H*)-one (7c). Light yellow oil, 45% yield. ^{1}H NMR ($CDCl_3$): δ = 8.15 (dd, 1H, J = 5.0, 1.5), 7.46–7.41 (m, 1H), 7.23–7.18 (m, 1H), 7.17–7.05 (m, 2H), 6.96 (t, 1H, J = 7.4), 6.62–6.55 (m, 2H), 3.98, (t, 2H, J = 7.4), 3.53–3.50 (m, 4H), 2.87–2.82 (m, 2H), 2.61–2.57 (m, 2H), 2.52 (t, 4H, J = 5.0), 2.44 (t, 2H, J = 7.1), 1.85 (q, 2H, J = 7.3); ^{13}C NMR ($CDCl_3$): δ = 170.6, 159.9, 148.3, 140.0, 137.8, 128.4, 127.8, 126.9, 123.1, 115.2, 113.7, 107.5, 56.1, 53.4, 45.6, 40.8, 32.3, 26.0, 25.0; IR (film): 2929, 2810, 1665, 1595, 1436, 1378, 1311, 1245; MS (EI), m/z 350 ([M]$^+$, 7.4), 256 (12), 231 (15), 188 (35), 107 (100); *Chlorhydrate*: white solid; mp: 229–231 °C; Anal. calcd for $C_{21}H_{26}N_4O{\cdot}HCl{\cdot}2.8H_2O$: C 57.67, H 7.51, N 12.81%, found: C 57.77, H 7.66, N 12.72%.

3,4-Dihydro-1-[3-(4-(2-pyrimidyl)piperazin-1-yl)propyl]quinolin-2(1*H*)-one (7d). Colorless oil, 42% yield. ^{1}H NMR ($CDCl_3$): δ = 8.27 (d, J = 4.7), 7.24–6.95 (m, 4H), 6.45 (t, 1H, J = 4.7), 3.99 (t, 2H, J = 7.4), 3.83–3.79 (m, 4H), 2.89–2.84 (m, 2H), 2.64–2.59 (m, 2H), 2.5–2.42 (m, 6H), 1.86 (q, 2H, J = 7.3); ^{13}C NMR ($CDCl_3$): δ = 170.6, 162.0, 158.1 (2C), 140.0, 128.4, 127.8, 126.9, 123.1, 115.26, 110.3, 56.1, 53.5 (2C), 44.0 (2C), 40.8, 32.3, 26.0, 25.0; IR (film): 2942, 2370, 1667, 1584, 1545, 1498, 1457, 1362, 1261; MS (EI), m/z 351 ([M]$^+$, 30), 231 (41), 188 (100); *Chlorhydrate*: white solid; mp: 215–216 °C; Anal. calcd for $C_{20}H_{25}N_5O{\cdot}HCl{\cdot}0.2C_3H_8O{\cdot}0.5H_2O$: C 55.55, H 6.70, N 15.72%, found: C 55.36, H 7.05, N 16.08%.

3,4-Dihydro-1-[3-(4-(2,3-dichlorophenyl)piperazin-1-yl)propyl]-quinolin-2(1*H*)-one (7f). Yellow oil, 48% yield. ^{1}H NMR ($CDCl_3$): δ = 7.26–7.08 (m, 4H), 7.02–6.93 (m, 3H), 4.04–3.99 (m, 2H), 3.08 (br s, 4H), 2.91–2.87 (m, 2H), 2.67–2.64 (m, 6H), 2.52 (t, 2H, J = 7.17), 1.89 (q, 2H, J = 7.32); ^{13}C NMR ($CDCl_3$): δ = 170.6, 151.6, 140.0, 133.4, 128.4, 127.9, 127.8, 126.9, 125.0, 123.1, 119.0, 115.2, 55.97, 53.6 (2C), 51.6 (2C), 40.8, 32.3, 26.0, 24.9; IR (film): 2948, 2822, 1711, 1665, 1598, 1580, 1499, 1454, 1377, 1270; MS (EI) m/z 431 ([M]$^+$, 0.5), 382 (9.3), 243 (100), 217 (56), 188 (64); *Chlorhydrate*: white solid; mp: 199–200 °C; Anal. calcd for: $C_{22}H_{26}Cl_2N_3O{\cdot}HCl{\cdot}0.7H_2O$: C 56.41, H 6.11, N 8.97%, found: C 56.32, H 5.94, N 9.00%.

4,5-Dihydro-1-[3-(4-(2-methoxyphenyl)piperazin-1-yl)propyl]-1*H*-benzo[*b*]azepin-2(3*H*)-one (8a). Yellow oil, 70% yield. ^{1}H NMR ($CDCl_3$): δ = 7.31–7.12 (m, 4H), 7.01–6.83 (m, 4H), 3.84 (s, 3H), 3.05 (br s, 4H), 2,71 (br s, 2H), 2,56 (br s, 4H), 2,39 (t, 2H, J = 7.4), 2.27 (t, 2H, J = 6.1), 2.17–2.04 (m, 2H), 1.84–1.77 (m, 4H); ^{13}C NMR ($CDCl_3$): δ = 173.3, 152.6, 142.8, 141.7, 136.3, 129.7, 127.9, 126.6, 123.2, 121.4, 118.6, 111.5, 56.3, 55.7, 53.7, 51.0, 46.4, 33.7, 30.6, 29.3, 26.0; IR (film): 2942, 2817, 1710, 1657, 1597, 1498, 1387, 1240; MS (EI) m/z 393 ([M]$^+$, 21), 378 (35), 205 (100), 190 (36), 120 (34); *Chlorhydrate*: white solid; mp: 202–205 °C (2-propanol); Anal. calcd for $C_{24}H_{31}N_3O_2{\cdot}HCl{\cdot}1.85H_2O$: C 62.22, H 7.77, N 9.07%, found: C 62.44, H 7.99, N 9.02%.

4,5-Dihydro-1-[3-(4-(2,3-dichlorophenyl)piperazin-1-yl)propyl]-1*H*-benzo[*b*]azepin-2(3*H*)-one (8f). Yellow oil, 63% yield. ^{1}H NMR ($CDCl_3$): δ = 7.31–7.11 (m, 6H), 7.09–6.8 (m, 1H), 3.01 (br s, 4H), 2.71 (br s, 2H), 2.55 (br s, 4H), 2.39 (t, 2H, J = 7.2), 2.25 (d, 2H, J = 6.1), 2.17 (br s, 2H), 1.84–1.77 (m, 2H); ^{13}C NMR ($CDCl_3$): δ = 173.3, 151.7, 142.8, 136.3, 134.4, 129.7, 128.5, 127.9, 127.8, 126.6, 124.9, 123.2, 119.0, 56.1, 53.5, 51.7, 46.4, 33.7, 30.6, 29.3, 26.0; IR (film): 2942, 2817, 1710, 1657, 1593, 1550, 1455, 1387, 1240; MS (EI) m/z 431 ([M]$^+$, 0.8), 396 (12), 243 (78), 202 (100); *Chlorhydrate*: white solid; mp: 234–236 °C (dec.); Anal. calcd for $C_{23}H_{27}Cl_2N_3O{\cdot}HCl{\cdot}0.4H_2O$: C 58.03, H 6.10, N 8.83%, found: C 58.21, H 6.32, N 8.85%.

Method B: general procedure for alkylation of benzolactams 2a–b and 3a with 1-bromo-4-chlorobutane

60% NaH (98 mg, 2.45 mmol) was slowly added to a stirred solution of the benzolactam (1.36 mmol) in anhydrous benzene (5 mL) under argon atmosphere, and the mixture was held at reflux for 1 h. After cooling to room temperature, 1-bromo-4-chlorobutane (0.3 mL, 2.7 mmol) was added dropwise, and the mixture continued to reflux for 72 h. The solvent was evaporated under reduced pressure, and the resulting residue was purified by silica gel chromatography (eluent: EtOAc/hexanes 1:1) to obtain the desired products as colorless oils, with the exception of **9b**, which crystal-

lized. This procedure was followed using 1-bromo-5-chloropentane instead of 1-bromo-4-chlorobutane to obtain chloropentylbenzolactam **10a**.

***N*-(4-Chlorobutyl)-3,4-dihydroisoquinolin-1(2*H*)-one (9a).** Yellow oil, 62% yield. ^{1}H NMR: ($CDCl_3$): δ = 8.05 (dd, 1H, J = 7.4, 1.3), 7.43–7.30 (m, 2H), 7.16 (d, 1H, J = 7.4), 3.63–3.53 (m, 6H), 2.98 (t, 2H, J = 6.6), 1.91–1.74 (m, 4H). Spectroscopic data agree with published values.[21]

***N*-(4-Chloropentyl)-3,4-dihydroisoquinolin-1(2*H*)-one (10a).** Yellow oil, 75% yield. ^{1}H NMR ($CDCl_3$): δ = 8.06 (dd, 1H, J = 7.5, 1.3), 7.43–7.30 (m, 2H), 7.16 (d, 1H, J = 7.3), 3.60–3.51 (m, 6H), 2.98 (t, 2H, J = 6.6), 1.87–1.61 (m, 2H), 1.55–1.51 (m, 2H), 1.49–1.45 (m, 2H); ^{13}C NMR ($CDCl_3$): δ = 164.4, 137.9, 131.5, 129.5, 128.2, 127.0, 126.8, 47.2, 46.1, 44.9, 32.2, 28.2, 27.0, 24.2; IR: 2933, 1644, 1604, 1480, 1422, 1308, 1262; MS (EI) *m/z* 251 ([*M*]$^+$, 9), 216 (14), 174 (12), 160 (100).

***N*-(4-Chlorobutyl)-1,2,3,4-tetrahydrobenzo[*c*]azepin-1-one (9b).** White solid, 70% yield; mp: 59–60 °C. Spectroscopic data agree with published values.[21]

***N*-(4-Chlorobutyl)-3,4-dihydroquinolin-2(1*H*)-one (11a).** Colorless oil, 59% yield. Spectroscopic data agree with published values.[38]

General Procedure for the *N*-alkylation of substituted piperazines with *N*-(ω-chloroalkyl)benzolactams 9a–11a and 9b. K_2CO_3 (0.42 g, 3 mmol) was slowly added to a solution of the substituted piperazine (0.84 mmol) in methylisobutylketone (5 mL) under argon atmosphere. The resulting suspension was held at reflux for 1 h. The *N*-(ω-chloroalkyl)benzolactam (0.42 mmol) and catalytic KI were added, and the mixture was held at reflux for a further 48 h. The solvent was evaporated under reduced pressure and the residue was extracted with H_2O and CH_2Cl_2. The combined organic layers were dried over Na_2SO_4 and concentrated under reduced pressure. The crude oil was purified by column chromatography (eluent: EtOAc/hexane → EtOAc) to afford the desired compound.

3,4-Dihydro-*N*-[4-(4-(2-methoxyphenyl)piperazin-1-yl)butyl]isoquinolin-1(2*H*)-one (12a). Yellow solid, 74% yield; mp: 107–108 °C (cyclohexane); *Chlorhydrate*: white solid; mp: 233–234 °C; Anal. calcd for $C_{24}H_{31}N_3O_2$·HCl: C 67.04, H 9.77, N 7.50%, found: C 67.05, H 7.75, N 9.60%. Spectroscopic data agree with published values.[14]

3,4-Dihydro-*N*-[4-(4-(4-methoxyphenyl)piperazin-1-yl)butyl]isoquinolin-1(2*H*)-one (12b). White solid, 40% yield; mp: 106–107 °C (cyclohexane). ^{1}H NMR ($CDCl_3$): δ = 8.07 (dd, 1H, J = 7.5, 1.3), 7.43–7.31 (m, 2H), 7.17 (d, 1H), 6.91–6.81 (m, 4H), 3.76 (s, 3H), 3.63–3.54 (m, 4H), 3.10 (t 4H, J = 4.9), 2.99 (t, 2H, J = 6.6), 2.63 (t, 4H, J = 4.9), 2.48–2.44 (m, 2H), 1.71–1.57 (m, 4H, J = 7.3); ^{13}C NMR ($CDCl_3$): δ = 164.8, 154.5, 146.2, 138.3, 131.9, 130.0, 128.6, 127.4, 127.2, 118.5, 114.8, 58.7, 56.0, 53.8, 51.0, 47.7, 46.4, 28.6, 26.1, 24.7; IR (KBr): 2934, 2825, 1645, 1512, 1243, 1034; MS (EI) *m/z* 365 ([*M*]$^+$, 7), 257 (52), 245 (55) 177 (100) 148 (62) 122 (63); *Chlorhydrate*: white solid; mp: 217–219 °C; Anal. calcd for $C_{24}H_{31}N_3O_2$·HCl: C 67.04, H 7.50, N 9.77%, found: C 66.83, H 7.80, N 9.70%.

3,4-Dihydro-*N*-[4-(4-(2-pyridyl)piperazin-1-yl)butyl]isoquinolin-1(2*H*)-one (12c). White solid, 30% yield; mp: 82–83 °C. ^{1}H NMR ($CDCl_3$): δ = 8.19–8.17 (m, 1H), 8.07 (d, 1H, J = 7.5), 7.49–7.3 (m, 3H), 7.6 (d, 1H, J = 7.4), 6.65–6.59 (m, 2H), 3.63–3.52 (m, 8H), 2.99 (t, 2H, J = 6.6), 2.55 (t, 4H, J = 5.1), 2.43 (t, 2H, J = 7.3), 1.72–1.60 (m, 4H); ^{13}C NMR ($CDCl_3$): δ = 164.5, 160.0, 148.34, 137.8, 131.9, 131.9, 130.0, 128.6, 127.4, 127.2, 113.6, 107.4, 58.8, 53.5, 47.6, 46.4, 45.6, 28.6, 26.1, 24.6; IR (KBr): 2932, 1646, 1435; MS (EI) *m/z* 364 ([*M*]$^+$, 5), 257 (23), 245 (43), 202 (41), 160 (50), 107 (100); Anal. calcd for $C_{22}H_{28}N_4O$·0.1 H_2O: N 15.3, C 72.14, H 7.76%, found: N 15.53, C 72.14, H 7.99%.

3,4-Dihydro-*N*-[4-(4-(2-pyrimidyl)piperazin-1-yl)butyl]isoquinolin-1(2*H*)-one (12d). Pale brown solid, 76% yield; mp: 100–102 °C (cyclohexane). ^{1}H NMR ($CDCl_3$): δ = 8.28 (dd, 2H, J = 4.5, 2.1), 8.05 (dd, 1H, J = 7.5, 1.3), 7.42–7.29 (m, 2H), 7.15 (d, 1H, J = 7.2), 6.46 (t, 1H, J = 4.7), 3.81 (t, 4H, J = 5.1), 3.61–3.52 (m, 4H), 2.97 (t, 2H, J = 6.6), 2.50 (t, 4H, J = 5.1), 2.43 (t, 2H, J = 7.2), 1.70–1.56 (m, 4H); ^{13}C NMR ($CDCl_3$): δ = 164.7, 161.9, 159.2, 138.3, 131.9, 129.9, 128.6, 127.4, 127.2, 110.2, 58.6, 53.4, 47.5, 46.4, 43.9, 28.6, 26.0, 24.4; IR (film): 2932, 1638, 1585, 1358; MS (EI) *m/z* 365 ([*M*]$^+$, 7), 257 (52), 177 (100), 148 (62); Anal. calcd for $C_{21}H_{27}N_5O$·0.85 H_2O: C 66.24, N 18.39, H 7.60%, found: C 66.52, N 18.72, H 7.44%.

3,4-Dihydro-*N*-[4-(4-(2,3-dichlorophenyl)piperazin-1-yl)butyl]isoquinolin-1(2*H*)-one (12f). Pale brown oil, 60% yield. ^{1}H NMR ($CDCl_3$): δ = 8.05 (dd, 1H, J = 7.7, 1.2), 7.45–7.21 (m, 2H), 7.22–7.13 (m, 3H), 6.98 (dd, 1H, J = 7.4, 2.2), 3.62 (t, 2H, J = 6.7), 3.57 (t, 2H, J = 6.7) 3.30 (t, 4H, J = 4.4), 3.01 (t, 4H, J = 6.6), 2.83 (d, 2H, J = 7.9), 1.83–1.71 (m, 4H); ^{13}C NMR ($CDCl_3$): δ = 164.8, 151.6, 138.3, 135.1, 132.1, 130.0, 128.5, 128.1, 127.5, 127.4, 125.7, 122.7, 119.4, 58.0, 53.2, 49.9, 46.7, 46.4, 28.6, 25.7, 20.1; IR (film): 2929, 2811, 1645, 1574, 1452; MS (EI) *m/z* 431 ([*M*]$^+$, 0.68), 243 (54), 231 (100), 160 (23); *Chlorhydrate*: white solid; mp: 211–212 °C; Anal. calcd for $C_{23}H_{27}Cl_2N_3O$·HCl·0.4 H_2O: N 8.96, C 58.92, H 6.02%, found: N 8.75, C 57.95, H 5.94%.

2-[4-(4-(2-Chlorophenyl)piperazin-1-yl)butyl)-3,4-dihydroisoquinolin-1(2*H*)-one (12g). Yellow–orange oil, 71% yield; *Chlorhydrate*: white solid; mp: 178–179 °C; Anal. calcd for $C_{23}H_{29}Cl_2N_3O$·HCl·0.25 H_2O: N 8.84, C 58.11, H 6.47%, found: N 9.05, C 57.90, H 6.21%. Spectroscopic data agree with published values.[14]

3,4-Dihydro-*N*-[4-(4-(3-methoxyphenyl)piperazin-1-yl)butyl]isoquinolin-1(2*H*)-one (12h). Orange oil, 75% yield. ^{1}H NMR ($CDCl_3$): δ = 8.06 (dd, 1H, J = 7.4, 1.1), 7.4–7.33 (m, 2H), 7.18–7.13 (m, 2H), 6.53 (dd, J = 8.2, 2.1), 6.46–6.38 (m, 2H), 3.78 (s, 3H), 3.62–3.53 (m, 4H), 3.2–3.17 (m, 4H), 2.98 (t, 2H, J = 6.6), 2.61–2.58 (m, 4H), 2.44 (t, 2H, J = 7.2), 1.68–1.57 (m, 4H); ^{13}C NMR ($CDCl_3$): δ = 164.3, 160.5, 152.7, 137.9, 131.5, 129.7, 129.6, 128.2, 127.0, 126.8, 108.8, 104.4, 102.4, 58.2, 55.1, 53.1, 48.9, 47.2, 46.0, 28.2, 25.7, 24.1; IR (film): 2940, 2822, 1750, 1720, 1667, 1498, 1490, 1380; MS (EI) *m/z* 393 ([*M*]$^+$, 23), 378 (30), 257 (21), 231 (100), 205 (68); *Chlorhydrate*: white solid; mp: 170–173 °C (dec.); Anal. calcd for $C_{24}H_{31}N_3O_2$·2 HCl·0.25 H_2O: N 8.92, C 61.21, H 7.17%, found: N 9.23, C 61.05, H 7.48%.

3,4-Dihydro-*N*-[5-(4-(2-methoxyphenyl)piperazin-1-yl)pentyl]isoquinolin-1(2*H*)-one (13a). Pale orange oil, 74% yield. ^{1}H NMR ($CDCl_3$): δ = 8.06 (dd, 1H, J = 7.6, 1.1), 7.38–7.28 (m, 6H), 7.14 (d, 1H, J = 7.2), 6.99–6.88 (m, 3H), 6.83 (d, 1H, J = 7.6), 3.84 (s, 3H), 3.58–3.51 (m, 4H), 3.09 (br s, 4H), 2.96 (t, 2H, J = 6.6), 2.65 (br s, 4H), 2.41 (t, 2H, J = 7.6), 1.68–1.54 (m, 4H); ^{13}C NMR ($CDCl_3$): δ = 164.6, 152.6, 141.7, 138.3, 131.8, 130.0, 128.6, 127.4, 127.2, 123.3, 121.4, 118.6, 111.6, 58.9, 55.7, 53.9, 53.8, 50.9, 47.7, 46.5, 28.6, 28.0, 27.3, 25.3; IR (film): 2936, 2819, 2369, 2252, 1644, 1601, 1446, 1307, 1241; MS (EI) *m/z* 407 ([*M*]$^+$, 6), 392 (20), 245 (77), 205 (100), 190 (38), 177 (17), 160 (50); *Chlorhydrate*: light yellow solid; mp: 195–197 °C; Anal. calcd for $C_{25}H_{33}N_3O_2$·2 HCl·0.5 H_2O: N 8.58, C 61.35, H 7.41%, found: N 8.51, C 61.34, H 7.41%.

2,3,4,5-Tetrahydro-*N*-[4-(4-(2-methoxyphenyl)piperazin-1-yl)butyl]benzo[*c*]azepin-1-one (14a). Yellow solid, 45% yield; mp: 107–

108 °C; *Chlorhydrate*: white solid; mp: 182–184 °C; Anal. calcd for $C_{25}H_{33}N_3O_2 \cdot HCl \cdot 1.95\,H_2O$: N 7.97, C 62.67, H 8.77%, found: N 8.79, C 62.48, H 7.70%. Spectroscopic data agree with published values.[14]

2,3,4,5-Tetrahydro-*N*-[4-(4-(4-methoxyphenyl)piperazin-1-yl)butyl]benzo[*c*]azepin-1-one (14b). White solid, 73% yield; mp: 91–92 °C (cyclohexane). ^{1}H NMR ($CDCl_3$): $\delta = 7.65$ (dd, 1H, $J = 7.2$, 1.8), 7.35–7.30 (m, 2H), 7.13–7.10 (m, 1H), 6.91–6.81 (m, 4H), 3.75 (s, 3H), 3.62–3.57 (m, 2H), 3.19 (t, 2H, $J = 6.4$), 3.10 (t, 4H, $J = 4.9$), 2.78 (t, 2H, $J = 7.1$), 2.61 (t, 4H, $J = 4.9$), 2.54–2.49 (m, 2H), 2.02 (q, 2H, $J = 6.7$), 1.73–1.60 (m, 4H); ^{13}C NMR ($CDCl_3$): $\delta = 171.4$, 154.2, 146.2, 137.6, 136.8, 131.1, 128.9, 128.5, 127.3, 118.5 (2C), 114.8 (2C), 58.7, 55.9, 53.8, 51.0, 47.6, 46.6, 30.7, 30.48, 24.7; IR (KBr): 2940, 2821, 1708, 1633, 1512, 1455, 1368, 1241; MS (EI) *m/z* 393 ([*M*]$^+$, 15), 378 (19), 231 (87), 202 (100), 162 (43), 135 (51), 120 (50); *Chlorhydrate*: white solid; mp: 234–236 °C; Anal. calcd for $C_{25}H_{33}N_3O_2 \cdot HCl \cdot 0.4\,CH_3OH$: N 9.46, C 67.63, H 7.72%, found: N 9.28, C 66.93, H 8.03%.

2,3,4,5-Tetrahydro-*N*-[4-(4-(2-pyridyl)piperazin-1-yl)butyl]benzo[*c*]azepin-1-one (14c). White solid, 49% yield; mp: 116–117 °C (cyclohexane). ^{1}H NMR ($CDCl_3$): $\delta = 8.19$–8.17 (m, 1H), 7.65 (dd, 1H, $J = 7.2$, 1.7), 7.49–7.44 (m, 1H), 7.36–7.30 (m, 2H), 7.14–7.11 (m, 1H), 6.65–6.59 (m, 2H), 3.62–3.53 (m, 6H, $J = 7.4$), 3.20 (t, 2H, $J = 6.4$), 2.78 (t, 2H, $J = 7.1$), 2.56 (t, 4H, $J = 5.1$), 2.45 (t, 2H, $J = 7.3$), 2.05–2.00 (m, 2H), 1.71–1.61 (m, 4H); ^{13}C NMR ($CDCl_3$): $\delta = 171.5$, 160.0, 148.3, 137.8, 137.6, 137.0, 131.0, 128.9, 128.5, 127.3, 113.6, 107.4, 58.8, 53.5, 46.6, 46.6, 45.7, 30.7, 30.49, 27.3, 24.7; IR (KBr): 2928, 1630, 1583, 1445, 1436, 1310; MS (EI) *m/z* 378 ([*M*]$^+$, 5), 259 (34), 216 (37), 174 (24), 123 (100); *Chlorhydrate*: white solid; mp: 206–207 °C (dec.); Anal. calcd for $C_{23}H_{30}N_4O \cdot 2\,HCl \cdot 0.65\,H_2O$: N 12.10, C 59.65, H 7.25%, found: N 12.10, C 59.59, H 7.25%.

2,3,4,5-Tetrahydro-*N*-[4-(4-(2-pyrimidyl)piperazin-1-yl)butyl]benzo[*c*]azepin-1-one (14d). Yellow oil, 28% yield. ^{1}H NMR ($CDCl_3$): $\delta = 8.28$ (d, 2H, $J = 4.8$), 7.25 (dd, 1H, $J = 7.2$, 1.8), 7.37–7.27 (m, 2H), 7.13–7.10 (m, 1H), 6.47 (t, 1H, $J = 4.8$), 3.85 (t, 4H, $J = 5.1$), 3.61–3.56 (m, 2H), 3.22 (t, 2H, $J = 6.4$), 2.76 (t, 2H, $J = 7.1$), 2.55 (t, 4H, $J = 5.1$), 2.51–2.46 (m, 2H), 2.06–1.97 (m, 2H), 1.70–1.61 (m, 4H); ^{13}C NMR ($CDCl_3$): $\delta = 171.4$, 162.0, 158.1, 137.6, 136.8, 131.1, 128.9, 128.5, 127.3, 110.2, 58.7, 53.4, 47.5, 46.6, 43.9, 30.6, 30.4, 27.3, 24.5; IR (film): 2937, 1627, 1585, 1548, 1448, 1356, 1246; MS (EI) *m/z* 379 ([*M*]$^+$, 6), 259 (52), 216 (44), 177 (100), 148 (47); *Chlorhydrate*: yellow solid; mp: 149–150 °C; Anal. calcd for $C_{22}H_{29}N_5O \cdot 2\,HCl \cdot 1.95\,H_2O$: N 14.36, C 54.2, H 7.21%, found: N 14.53, C 54.03, H 7.20%.

2,3,4,5-Tetrahydro-*N*-[4-(4-(2,3-dichlorophenyl)piperazin-1-yl)butyl]benzo[*c*]azepin-1-one (14f). Colorless oil, 51% yield; *Chlorhydrate*: yellow solid; mp: 192–193 °C (EtOAc); Anal. calcd for $C_{24}H_{29}Cl_2N_3O \cdot HCl \cdot 1.25\,H_2O$: N 8.31, C 57.04, H 6.48%, found: N 8.42, C 57.16, H 6.65%. Spectroscopic data agree with published values.[14]

3,4-Dihydro-*N*-[4-(4-(2-methoxyphenyl)piperazin-1-yl)butyl]quinolin-2(1*H*)-one (15a); *Chlorhydrate*: off-white solid; mp: 198–199 °C. Spectroscopic data agree with published values.[37]

3,4-Dihydro-*N*-[4-(4-(4-methoxyphenyl)piperazin-1-yl)butyl]quinolin-2(1*H*)-one (15b). Yellow oil, 51% yield. ^{1}H NMR ($CDCl_3$): $\delta =$ 7.22–7.14 (m, 2H), 7.07–6.99 (m, 2H), 6.92–6.82 (m, 4H), 3.99–3.94 (m, 2H), 3.76 (s, 3H), 3.12–3.09 (m, 4H), 2.91–2.86 (m, 2H), 2.66–2.61 (m, 6H), 2.46 (t, 2H, $J = 7.16$), 1.72–1.59 (m, 4H); ^{13}C NMR ($CDCl_3$): $\delta = 170.6$, 154.2, 146.1, 139.9, 128.4, 127.8, 127.0, 123.1, 118.6 (2C), 115.3, 114.8 (2C), 58.9, 56.0, 53.6 (2C), 50.9 (2C), 42.2, 32.3, 26.0, 25.3, 24.2; IR (film): 1932, 2370, 1660, 1511, 1459, 1379, 1242; MS (EI) *m/z* 393 ([*M*]$^+$, 37), 378 (13), 231 (31), 205 (100); *Chlorhydrate*: white solid; mp: 181–182 °C; Anal. calcd for $C_{24}H_{31}N_3O_2 \cdot HCl \cdot 0.7\,H_2O$: C 60.17, H 7.24, N 8.77%, found: C 60.03, H 7.01, N 8.87%.

3,4-Dihydro-*N*-[4-(4-(2-pyridyl)piperazin-1-yl)butyl]quinolin-2(1*H*)-one (15c). Yellow oil, 87% yield. ^{1}H NMR ($CDCl_3$): $\delta = 8.18$–8.17 (m, 1H), 7.49–7.44 (m, 1H), 7.22 (t, 2H, $J = 7.8$), 7.17–7.05 (m, 2H), 6.65–6.59 (m, 2H), 3.97 (t, 2H, $J = 7.4$), 3.56–3.53 (m, 4H), 2.91–2.86 (m, 2H), 2.66–2.60 (m, 2H), 2.56–2.53 (m, 4H), 2.45–2.40 (m, 2H), 1.76–1.61 (m, 4H); ^{13}C NMR ($CDCl_3$): $\delta = 170.5$, 159.9, 148.3, 139.9, 137.8, 128.4, 127.8, 127.0, 123.0, 115.3, 113.7, 107.4, 58.3, 53.4(2C), 45.6 (2C), 42.2, 25.9, 25.3, 24.3; IR (film): 2935, 1650, 1437, 1300; MS (EI) *m/z* 64 ([*M*]$^+$, 37); *Chlorhydrate*: white solid; mp: 202–204 °C; Anal. calcd for $C_{22}H_{28}N_4O \cdot 3\,HCl \cdot 0.35\,H_2O$: C 55.03, H 6.65, N 11.67%, found: C 54.8, H 6.99, N 12.09%.

3,4-Dihydro-*N*-[4-(4-(2-pyrimidyl)piperazin-1-yl)butyl]quinolin-2(1*H*)-one (15d). Yellow oil, 80% yield. ^{1}H NMR ($CDCl_3$): $\delta = 8.29$ (d, 2H, $J = 4.7$), 7.22 (t, 1H, $J = 7.2$), 7.15 (d, 1H, $J = 7.2$), 7.05 (d, 1H, $J = 8.1$), 6.98 (t, 1H, $J = 7.4$), 6.46 (t, 1H, $J = 4.7$), 3.98–3.93 (m, 2H), 3.82 (t, 4H, $J = 5.05$), 2.90–2.85 (m, 2H), 2.63–2.60 (m, 2H), 2.48 (t, 4H, $J = 5.1$), 2.41 (t, 2H, $J = 7.2$), 1.73–1.57 (m, 4H); ^{13}C NMR ($CDCl_3$): $\delta = 170.5$, 162.0, 158.1 (2C), 139.9, 128.41, 127.8, 127.0, 123.1, 115.3, 110.2, 58.3, 53.4 (2C), 44.0 (2C), 42.2, 32.3, 26.0, 25.3, 24.3; IR (film): 2937, 2370, 1668, 1585, 1546, 1457, 1360, 1263; MS (EI) *m/z* 365 ([*M*]$^+$, 12), 257 (42), 245 (38), 177 (100), 148 (50); *Chlorhydrate*: white solid; mp: 153–154 °C; Anal. calcd for $C_{21}H_{27}N_5O \cdot 2\,HCl \cdot 1.8\,H_2O$: C 53.57, H 6.98, N 14.87%, found: C 53.42, H 6.90, N 15.12%.

3,4-Dihydro-*N*-[4-(4-(2,3-dichlorophenyl)piperazin-1-yl)butyl]quinolin-2(1*H*)-one (15f). Light yellow solid, 88% yield; mp: 93–95 °C. ^{1}H NMR ($CDCl_3$): $\delta = 7.24$–6.93 (m, 7H), 3.99–3.95 (m, 2H), 3.06 (br s, 4H), 2.91–2.87 (m, 2H), 2.67–2.62 (m, 6H), 2.47 (t, 2H, $J = 7.1$), 1.77–1.61 (m, 4H); ^{13}C NMR ($CDCl_3$): $\delta = 171.3$, 152.0, 139.5, 128.4, 127.8, 127.8, 124.9, 123.1, 119.0, 115.3, 58.2, 53.6, 51.7, 42.3, 32.3, 26.0, 25.4, 24.4; IR (KBr): 2948, 2822, 1709, 1667, 1496, 1454; MS (EI) *m/z* 459 ([*M*]$^+$, 0.6) 382 (6), 243 (100); Anal. calcd for $C_{23}H_{27}Cl_2N_3O$: C 63.89, H 6.30, N 9.72%, found: C 63.73, H 6.40, N 9.61%.

Pharmacology

Radioligand binding competition assays. Radioligand binding competition assays were performed in vitro using human D_2 and D_3 receptors transfected in CHO cells. Further details are provided below.

Human D_2 receptors. Dopamine D_2 receptor competition binding experiments were carried out in membranes from CHO-D_2 cells. On the day of the assay, membranes were defrosted and re-suspended in binding buffer (50 mM Tris-HCl, 120 mM NaCl, 5 mM KCl, 5 mM $MgCl_2$, 1 mM EDTA, pH 7.4). Each reaction well of a 96-well plate, prepared in duplicate, contained 30 μg of protein, 0.2 nM [^{3}H]spiperone, and compounds in various of concentrations. Non-specific binding was determined in the presence of 10 μM sulpiride. The reaction mixture was incubated at 25 °C for 120 min, after which samples were transferred to a multiscreen FC 96-well plate (Millipore, Madrid, Spain), filtered, and washed four times with 250 μL wash buffer (50 mM Tris-HCl, 0.9% NaCl, pH 7.4), before measuring in a microplate beta scintillation counter (Microbeta Trilux, PerkinElmer, Madrid, Spain).

Human D_3 receptors. Dopamine D_3 receptor competition binding experiments were carried out in membranes from CHO-D_3 cells. On

the day of the assay, membranes were defrosted and re-suspended in binding buffer (50 mM Tris-HCl, 150 mM NaCl, 5 mM KCl, 5 mM $MgCl_2$, 5 mM EDTA, 1.5 mM $CaCl_2$, pH 7.4). Each reaction well of a 96-well plate, prepared in duplicate, contained 50 μg of protein, 1 nM [^{3}H]spiperone and compounds in various concentrations. Nonspecific binding was determined in the presence of 1 μM haloperidol. The reaction mixture was incubated at 25 °C for 60 min, after which samples were transferred to a multiscreen FB 96-well plate (Millipore, Madrid, Spain), filtered, and washed six times with 250 μL wash buffer (50 mM Tris-HCl, 0.9% NaCl, pH 7.4), before measuring in a microplate beta scintillation counter (Microbeta Trilux, PerkinElmer, Madrid, Spain).

Data analysis. The −log of the inhibition constant (pK_i) of each compound was calculated using the Cheng–Prusoff equation [Eq (1)]:

$$K_i = IC_{50}/(1 + [L]/K_d) \quad (1)$$

for which IC_{50} is the concentration of compound that displaces the binding of radioligand by 50%, [L] is the free concentration of radioligand, and K_d is the dissociation constant of each radioligand. IC_{50} values were obtained by fitting the data with nonlinear regression using Prism 2.1 software (GraphPad, San Diego, CA, USA). For those compounds that exhibited either low affinity or poor solubility, a percentage of inhibition of specific binding at 1 μM is reported. Results are the mean of three experiments ($n = 3$) each performed in duplicate.

Numbering of residues

For residues belonging to helix regions of the G-protein-coupled receptors (GPCRs), the generalized numbering scheme proposed by Ballesteros and Weinstein[39] was used.

GPCR modeling

Human sequences of the dopamine D_2 and D_3 receptors were retrieved from the Swiss-Prot database.[40] ClustalX software[41,42] was used to align these sequences with the crystal structure of the human β_2 adrenergic G-protein-coupled receptor (PDB entry 2RH1)[43,44] using the PAM250 matrix and penalties of 10 and 0.05, respectively, for "gap open" and "gap elongation." The resulting alignment was then manually refined to ensure perfect alignment of the highly conserved residues of the GPCR superfamily, according to Baldwin et al.[45] The conserved disulfide bond between residue Cys3.25 at the beginning of TM3 and the cysteine in the middle of the extracellular loop 2 (a feature common to many GPCR receptors) was also built and maintained as a constraint for geometric optimization. The structural models of the receptors were built using the MODELLER suite of programs,[46] which yielded 15 candidate models for each final receptor structure. The best structures were selected from these candidates, according to the MODELLER objective function and visual inspection. The resulting receptor structures were optimized by the Amber99 force field[47] using the molecular modeling program MOE (Molecular Operating Environment; Chemical Computing Group, Inc). PROCHECK software[48] was used to assess the stereochemical quality of the minimized structures, resulting in good quality parameters and an excellent distribution of Ψ and Φ angles in the Ramachandran plot (more than 90% of the residues are in the most favored regions). Additionally, the resulting models were superimposed with the template in order to reproduce the correct orientation of the side chains for the set of highly conserved amino acids in the GPCR superfamily,[49–52] paying special attention to the side chains of residues Phe6.51, Phe6.52 and Trp6.48, which according to some authors,[53] are involved in the activation process. In recently published data for 2RH1,[43,44] a co-crystallized partial inverse agonist, carazolol, interacts with Phe6.51 and Phe6.52, which form an extended aromatic network surrounding Trp6.48. As a result, the side chain of Trp6.48 adopts the rotamer associated with the inactive state. For our purposes, the conformation of these residues was set in the "inactive state", which is likely to be more appropriate for modeling the docking of antagonists and more consistent with the inactive state of the main template structure (2RH1).

Ligand geometries

Molecular structures were modeled in 2D, then converted to 3D using Corina v. 2.4.[54] The basic aliphatic nitrogen atom of the piperazine ring was assumed to be protonated at physiological conditions and modeled accordingly. Partial atomic charges were calculated with the Protonated 3D method implemented in MOE.

Docking simulations

Complexes for each of the compounds in the series with the dopamine D_2 and D_3 receptors were obtained via docking simulations with the GOLD 3.1.1 program.[55] The ligands were docked into the active site of D_2 and D_3 receptors by defining a 15 Å region centered on the CG of Asp3.32, a residue conserved in all aminergic receptors and known to be important for ligand interaction.[56,57] The best docking solution, according to the GoldScore scoring function of GOLD and mutagenesis data, was subjected to energy minimization using MOE. The complex was further refined by 200 ps molecular dynamics simulations (force field MMF94x, 300 K, time step 2 fs) and subsequently energy-minimized by applying gradient minimization until the RMS gradient was lower than 0.001 kcal mol^{-1}Å.

3D-QSAR analysis

The complete series was imported into Pentacle[58] for computing GRIND-2 molecular descriptors,[23] using the structures obtained from the previous docking simulations. For every compound in the series, we computed Molecular Interaction Fields (MIF) to represent the hydrophobic (DRY), hydrogen bond acceptor (O) and hydrogen bond donor (N1) properties, using a grid step of 0.5 Å. The structures of the compounds were also described using the TIP pseudoprobe. The resulting MIF were made discrete by using the AMANDA hotspot recognition method[23] with standard settings. Because the compounds had already been aligned, the new Consistently Large Auto and Cross-Correlation (CLACC) encoding[59] was used in place of the standard MACC encoding algorithm, with the aim of describing the spatial distribution of the hotspots by choosing pairs of grid nodes separated by a specific distance range or "bin." For every distance bin, if such a pair of nodes are found, the method annotates the product of their MIF energies, using a value of zero if these coupled nodes are not present. When more than one candidate couple is found, the MACC algorithm selects the one with a higher product, while the new algorithm used herein (CLACC) prioritizes pairs representing the same region of the space for the largest possible fraction of the series under analysis. As a result, the obtained descriptors are much more consistent than the classical GRIND,[24] resulting in better models in terms of predictive ability and interpretability.

The GRIND-2 descriptors, obtained as described above, were used to build partial least squares (PLS) models. These models were used to evaluate the affinity for D_2 (M1) and D_3 (M2) receptors, using the built-in modeling and variable selection tools available in Pentacle. For 3D-QSAR analysis purposes, inactive compounds were assigned an arbitrary pK_i value of 5. The binding affinities were translated to a logarithmic scale and the GRIND-2 descriptors were used, centered and with no scaling. The optimum number of PLS latent variables (LV) was assessed by the leave-one-out (LOO) cross-validation test. In both cases, a mild variable selection was applied using up to two sequential runs of the GOLPE-FFD methodology.[60] For the variable selection, two LVs were used, and those variables with uncertain effects on the model's predictive ability were not removed. All models were submitted to standard LOO cross-validation. The results of these analyses, using the optimum number of LV, were reported in Table 4. In addition, we carried out two stricter cross-validation tests (5RG and 2RG), which involve randomly splitting the series into either two (2RG) or five groups (5RG), which are removed and predicted in turn until every group has been removed once. The entire procedure is then repeated either 20 (for the 5RG method) or 100 (for the 2RG method) times to obtain q^2 values of 0.57 (M1, 5RG), 0.42 (M1, 2RG), 0.77 (M2, 5RG) and 0.64 (M2, 2RG), all of which are within close range of the values reported in Table 4. To further validate these models, and to estimate their true predictive ability, the series were split into training and test sets. The objects assigned to the test set (seven structures; 19% of the total series) were selected as representative compounds, both in terms of structure and biological response. Next, the entire 3D-QSAR modeling procedure was carried out as described above (PLS modeling and FFD variable selection) using only the compounds of the training set, while the compounds in the test set were used only as predictors. The Standard Deviation of Error of Prediction (SDEP) obtained for the test set was 0.44 for M1 and 0.57 for M2, and the external r^2 between experimental and predicted values was 0.93 for M1 and 0.82 for M2. These values are similar to those obtained by standard cross-validation methods and further confirm the accurate predictive ability of the models.

Finally, we built a PLS discriminant analysis (PLS-DA) model to describe D_3 receptor selectivity. In this model, a binary dependent variable discriminates between D_3 receptor selective and nonselective compounds. This variable was computed only for compounds with a pK_i for the D_3 receptor greater than 6, and was assigned values of 0 and 1 when the $pK_iD_3 - pK_iD_2$ value was >0.62 or <0.62, respectively. This cutoff value was assigned in order to reproduce an expert classification of the compounds in these two categories. Details of the PLS-DA model building and variable selection for this model are identical to those described above for the standard PLS models. However, because this model was built mainly for the purpose of summarizing the results of M1 and M2, using a smaller series, it was not subjected to any additional validation tests.

Acknowledgements

This work was supported in part by grants from the CICYT (Spain, SAF2005-08025-C03 and SAF2009-13609-C04) and by the Xunta de Galicia (Spain, PIDIT06PXIB203173PR and INCITE09 203 184 PR), as well as by the HERACLES (RD06/0009) and COMBIOMED (RD07/0067) RETIC networks from the Instituto de Salud Carlos III. GRIB is a node of the Spanish National Institute of Bioinformatics.

Keywords: 3D-QSAR · antipsychotics · benzolactams · D_2/D_3 selectivity · dopamine receptors

[1] D. M. Jackson, A. Westlind-Danielsson, *Pharmacol. Ther.* **1994**, *64*, 291 – 370.
[2] C. Missale, S. R. Nash, S. W. Robinson, M. Jaber, M. G. Caron, *Physiol. Rev.* **1998**, *78*, 189 – 225.
[3] P. Sokoloff, B. Giros, M. P. Martres, M. L. Bouthenet, J. C. Schwartz, *Nature* **1990**, *347*, 146 – 151.
[4] F. Boeckler, H. Lanig, P. Gmeiner, *J. Med. Chem.* **2005**, *48*, 694 – 709.
[5] B. Levant, *Pharmacol. Rev.* **1997**, *49*, 231 – 252.
[6] E. V. Gurevich, Y. Bordelon, R. M. Shapiro, S. E. Arnold, R. E. Gur, J. N. Joyce, *Arch. Gen. Psychiatry* **1997**, *54*, 225 – 232.
[7] C. Schmauss, V. Haroutunian, K. L. Davis, M. Davidson, *Proc. Natl. Acad. Sci. USA* **1993**, *90*, 8942 – 8946.
[8] J. C. Schwartz, J. Diaz, C. Pilon, P. Sokoloff, *Brain Res. Rev.* **2000**, *31*, 277 – 287.
[9] J. N. Joyce, M. J. Millan, *Drug Discovery Today* **2005**, *10*, 917 – 925.
[10] M. M. Marcus, K. E. Jardemark, M. Wadenberg, X. Langlois, P. Hertel, T. H. Svensson, *Int. J. Neuropsychopharmacol.* **2005**, *8*, 315 – 327.
[11] M. J. Millan, F. Loiseau, A. Dekeyne, A. Gobert, G. Flik, T. I. Cremers, J. Rivet, D. Sicard, R. Billiras, M. Brocco, *J. Pharmacol. Exp. Ther.* **2007**, *324*, 1212 – 1226.
[12] B. Kiss, I. Laszlovszky, A. Horváth, Z. Némethy, E. Schmidt, G. Bugovics, K. Fazekas, I. Gyertyán, E. Agai-Csongor, G. Domány, Z. Szombathelyi, *Naunyn-Schmiedeberg's Arch. Pharmacol.* **2008**, *378*, 515 – 528.
[13] L. Bettinetti, K. Schlotter, H. Hübner, P. Gmeiner, *J. Med. Chem.* **2002**, *45*, 4594 – 4597.
[14] R. Ortega, E. Raviña, C. F. Masaguer, F. Areias, J. Brea, M. I. Loza, L. López, J. Selent, M. Pastor, F. Sanz, *Bioorg. Med. Chem. Lett.* **2009**, *19*, 1773 – 1778.
[15] M. Tomita, S. Minami, S. Uyeo, *J. Chem. Soc. C* **1969**, 183 – 188.
[16] R. Conley, *J. Org. Chem.* **1958**, *23*, 1330 – 1333.
[17] D. Evans, I. Lockhart, *J. Chem. Soc.* **1965**, 4806 – 4812.
[18] G. Grunewald, V. Dahanukar, *J. Heterocycl. Chem.* **1994**, *31*, 1609 – 1617.
[19] U. R. Mach, A. E. Hackling, S. Perachon, S. Ferry, C. G. Wermuth, J. Schwartz, P. Sokoloff, H. Stark, *ChemBioChem* **2004**, *5*, 508 – 518.
[20] A. Hackling, R. Ghosh, S. Perachon, A. Mann, H. Höltje, C. G. Wermuth, J. Schwartz, W. Sippl, P. Sokoloff, H. Stark, *J. Med. Chem.* **2003**, *46*, 3883 – 3899.
[21] M. H. Norman, G. C. Rigdon, F. Navas, B. R. Cooper, *J. Med. Chem.* **1994**, *37*, 2552 – 2563.
[22] J. Selent, L. López, F. Sanz, M. Pastor, *ChemMedChem* **2008**, *3*, 1194 – 1198.
[23] A. Durán, G. C. Martínez, M. Pastor, *J. Chem. Inf. Model.* **2008**, *48*, 1813 – 1823.
[24] M. Pastor, G. Cruciani, I. McLay, S. Pickett, S. Clementi, *J. Med. Chem.* **2000**, *43*, 3233 – 3243.
[25] K. Ehrlich, A. Götz, S. Bollinger, N. Tschammer, L. Bettinetti, S. Härterich, H. Hübner, H. Lanig, P. Gmeiner, *J. Med. Chem.* **2009**, *52*, 4923 – 4935.
[26] E. M. Parker, D. A. Grisel, L. G. Iben, R. A. Shapiro, *J. Neurochem.* **1993**, *60*, 380 – 383.
[27] R. A. Glennon, M. Dukat, R. B. Westkaemper, A. M. Ismaiel, D. G. Izzarelli, E. M. Parker, *Mol. Pharmacol.* **1996**, *49*, 198 – 206.
[28] D. Fu, J. A. Ballesteros, H. Weinstein, J. Chen, J. A. Javitch, *Biochemistry* **1996**, *35*, 11278 – 11285.
[29] M. Arakawa, N. Yanamala, J. Upadhyaya, A. Halayako, J. Klein-Seetharaman, P. Chelikani, *Protein Sci.* **2010**, *19*, 85 – 93.
[30] Y. Sugimoto, R. Fujisawa, R. Tanimura, A. L. Lattion, S. Cotecchia, G. Tsujimoto, T. Nagao, H. Kurose, *J. Pharmacol. Exp. Ther.* **2002**, *301*, 51 – 58.
[31] K. Lundstrom, M. P. Turpin, C. Large, G. Robertson, P. Thomas, X. Q. Lewell, *J. Recept. Signal Transduction Res.* **1998**, *18*, 133 – 150.
[32] A. H. Newman, P. Grundt, G. Cyriac, J. R. Deschamps, M. Taylor, R. Kumar, D. Ho, R. R. Luedtke, *J. Med. Chem.* **2009**, *52*, 2559 – 2570.
[33] B. Lee, S. Chu, I. Lee, B. Lee, C. Song, D. Chi, *Bull. Korean Chem. Soc.* **2000**, *21*, 860 – 866.

[34] W. Malinka, M. Sieklucka-Dziuba, G. Rajtar, A. Rubaj, Z. Kleinrok, *Farmaco* **1999**, *54*, 390 – 401.
[35] W. Malinka, M. Kaczmarz, B. Filipek, J. Sapa, B. Glod, *Farmaco* **2002**, *57*, 737 – 746.
[36] L. Santana, E. Uriarte, Y. Fall, M. Teijeira, C. Terán, E. García-Martínez, B. Tolf, *Eur. J. Med. Chem.* **2002**, *37*, 503 – 510.
[37] J. L. Mokrosz, B. Duszyńska, M. H. Paluchowska, *Arch. Pharm.* **1994**, *327*, 529 – 531.
[38] H. Geneste, G. Backfisch, W. Braje, J. Delzer, A. Haupt, C. W. Hutchins, L. L. King, W. Lubisch, G. Steiner, H. Teschendorf, L. Unger, W. Wernet, *Bioorg. Med. Chem. Lett.* **2006**, *16*, 658 – 662.
[39] J. Ballesteros, H. Weinstein, *Methods Neurosci.* **1995**, *25*, 366 – 428.
[40] B. Boeckmann, A. Bairoch, R. Apweiler, M. Blatter, A. Estreicher, E. Gasteiger, M. J. Martin, K. Michoud, C. O'Donovan, I. Phan, S. Pilbout, M. Schneider, *Nucleic Acids Res.* **2003**, *31*, 365 – 370.
[41] J. D. Thompson, D. G. Higgins, T. J. Gibson, *Nucleic Acids Res.* **1994**, *22*, 4673 – 4680.
[42] J. D. Thompson, T. J. Gibson, F. Plewniak, F. Jeanmougin, D. G. Higgins, *Nucleic Acids Res.* **1997**, *25*, 4876 – 4882.
[43] V. Cherezov, D. M. Rosenbaum, M. A. Hanson, S. G. F. Rasmussen, F. S. Thian, T. S. Kobilka, H. Choi, P. Kuhn, W. I. Weis, B. K. Kobilka, R. C. Stevens, *Science* **2007**, *318*, 1258 – 1265.
[44] S. G. F. Rasmussen, H. Choi, D. M. Rosenbaum, T. S. Kobilka, F. S. Thian, P. C. Edwards, M. Burghammer, V. R. P. Ratnala, R. Sanishvili, R. F. Fischetti, G. F. X. Schertler, W. I. Weis, B. K. Kobilka, *Nature* **2007**, *450*, 383 – 387.
[45] J. M. Baldwin, G. F. Schertler, V. M. Unger, *J. Mol. Biol.* **1997**, *272*, 144 – 164.
[46] A. Sali, T. L. Blundell, *J. Mol. Biol.* **1993**, *234*, 779 – 815.
[47] W. Cornell, P. Cieplak, C. Bayly, I. Gould, K. Merz, D. Ferguson, D. Sepellmeyer, *J. Am. Chem. Soc.* **1995**, *117*, 5179 – 5197.
[48] R. Laskowski, M. MacArthur, D. Moss, J. Thornton, *J. Appl. Crystallogr.* **1993**, *26*, 283 – 291.
[49] J. A. Ballesteros, A. D. Jensen, G. Liapakis, S. G. Rasmussen, L. Shi, U. Gether, J. A. Javitch, *J. Biol. Chem.* **2001**, *276*, 29171 – 29177.
[50] C. Bissantz, *J. Recept. Signal Transduction Res.* **2003**, *23*, 123 – 153.
[51] D. A. Shapiro, K. Kristiansen, D. M. Weiner, W. K. Kroeze, B. L. Roth, *J. Biol. Chem.* **2002**, *277*, 11441 – 11449.
[52] I. Sylte, A. Bronowska, S. G. Dahl, *Eur. J. Pharmacol.* **2001**, *416*, 33 – 41.
[53] L. Shi, G. Liapakis, R. Xu, F. Guarnieri, J. A. Ballesteros, J. A. Javitch, *J. Biol. Chem.* **2002**, *277*, 40989 – 40996.
[54] J. Gasteiger, C. Rudolph, J. Sadowski, *Tetrahedron Comp. Method.* **1990**, *3*, 537 – 547.
[55] M. L. Verdonk, J. C. Cole, M. J. Hartshorn, C. W. Murray, R. D. Taylor, *Proteins* **2003**, *52*, 609 – 623.
[56] A. Mansour, F. Meng, J. H. Meador-Woodruff, L. P. Taylor, O. Civelli, H. Akil, *Eur. J. Pharmacol.* **1992**, *227*, 205 – 214.
[57] C. D. Wang, T. K. Gallaher, J. C. Shih, *Mol. Pharmacol.* **1993**, *43*, 931 – 940.
[58] Pentacle v. 1.05, Molecular Discovery Ltd., UK, **2009**.
[59] A. Durán, L. López, M. Pastor, *unpublished results*.
[60] M. Baroni, G. Costantino, G. Cruciani, D. Riganelli, R. Valigi, S. Clementi, *Quant. Struct–Act. Relat.* **1993**, *12*, 9 – 20.

Received: March 10, 2010
Revised: May 10, 2010
Published online on June 11, 2010

